Title: U-Th dating of carbonate crusts reveals Neanderthal origin of Iberian cave art

Authors: D. L. Hoffmann[1,*], C. D. Standish[2,*], M. García-Diez[3], P. B. Pettitt[4], J. A. Milton[5], J. Zilhão[6,7], J.J. Alcolea-González[8], P. Cantalejo-Duarte[9], H. Collado[10], R. de Balbín[8], M. Lorblanchet[11], J. Ramos-Muñoz[12], G.-Ch. Weniger[13,14], A. W. G. Pike[2,¥]

Affiliations:

[1]Max Planck Institute for Evolutionary Anthropology, Department of Human Evolution, Deutscher Platz 6, 04103 Leipzig, Germany

[2]Department of Archaeology, University of Southampton, Avenue Campus, Highfield Road, Southampton, SO17 1BF, UK.

[3]Faculty of Humanities and Social Sciences, University of Isabel I, c/ Fernán González 76, 09003 Burgos, Spain

[4]Department of Archaeology, Durham University, South Road, Durham, DH1 3LE, UK.

[5]Ocean and Earth Science, University of Southampton Waterfront Campus, National Oceanography Centre Southampton, European Way, Southampton SO14 3ZH, UK.

[6]University of Barcelona, Departament d'Història i Arqueologia (SERP), c/ Montalegre 6, 08001 Barcelona, Spain.

[7]Institució Catalana de Recerca i Estudis Avançats (ICREA), Passeig Lluís Companys 23, 08010 Barcelona, Spain

[8]Prehistory Section, University of Alcalá de Henares, c/ Colegios 2, 28801 Alcalá de Henares, Madrid, Spain

[9]Centro de la Prehistoria/Cueva de Ardales. Avda. de Málaga, nº 1. 29550 Ardales (Málaga), Spain.

[10]Quaternary-Prehistory Research Group, I-PAT Research Group, D.G. Bibliotecas, Museos y Patrimonio Cultural, Junta de Extremadura, Spain

[11]Directeur de recherches au CNRS-Retraité, Roc des Monges, 46200 St Sozy, France

[12]Departamento de Historia, Geografía y Filosofia, Universidad de Cádiz, Avda. Gómez Ulla s.n, Cádiz, Spain

[13]Neanderthal Museum, Talstraße 300, 40822 Mettmann

[14]Institute of Prehistory, University of Cologne, Germany

[*]These authors contributed equally to this study

[¥]Corresponding author: a.w.pike@soton.ac.uk

One sentence summary: U-Th dates on carbonate crusts overlying pigment at three sites in Spain demonstrate that Neanderthals were making cave paintings at least 64,800 years ago.

Abstract: The extent and nature of symbolic behaviour among Neanderthals is obscure. While evidence for Neanderthal body ornamentation has been proposed, all cave painting has been attributed to modern humans. Here we present dating results for three sites in Spain which show that cave art emerged in Iberia significantly earlier than previously known. U-Th dates on carbonate crusts overlying paintings provide minimum ages for a red linear motif in La Pasiega (Cantabria), a hand stencil in Maltravieso (Extremadura), and red-painted speleothems in Ardales (Andalusia). Collectively, these results show that cave art in Iberia is older than 64.8 ka. The earliest dated so far, this cave art pre-dates by at least 20 ka the arrival of modern humans in Europe, which implies Neanderthal authorship.

Main text: The origin of human symbolism is a central concern of modern Palaeoanthropology (*1*). For the European Middle Palaeolithic and the African Middle Stone Age, symbolic behaviour has been inferred from the use, presumably for body adornment, of mineral pigments, shell beads, eagle talons, and feathers (*2-7*). Cave and rock art constitutes particularly impressive and important evidence for symbolic behaviour (*8*), but little is known about the chronology of its emergence due to difficulties in dating it precisely and accurately (*9*).

Claims for Neanderthal authorship of cave art have been made (*10, 11*). However, ambiguities of indirect dating and uncertainty in distinguishing between natural and intentional modification (*12, 13*) leave these claims unresolved. Recent technical developments provide the possibility to obtain age constraints for cave art by U-Th dating of associated carbonate precipitates (*14*). This dating approach can provide robust age constraints while keeping the art itself intact. It is a destructive technique, in that a carbonate sample is required, although the sample is very small, typically less than 10 mg, and is taken not from the art itself, but from the carbonates associated with it. The key condition is demonstrating an unambiguous stratigraphic relationship between the sample and the art whose age we wish to constrain. Dating of carbonate crusts formed on top of the art provides a minimum age (*15*). When the art was painted on top of carbonates (e.g. on flowstone walls, stalagmites or stalactites), dating the underlying 'canvas' provides a maximum age (*15*).

Using this approach, the earliest results so far are for a hand stencil from Leang Timpuseng, Sulawesi (Indonesia), with a minimum age of 39.9 ka (*16*), and a red disc on the Panel of Hands in El Castillo, Cantabria (Spain), with a minimum age of 40.8 ka (*17*). While the art in Sulawesi has been attributed to modern humans, the minimum age for the red disc in El Castillo relates

to a point in time when it could be attributed either to Cantabria's first modern humans or to the region's earlier Neanderthal populations (*18, 19*).

Here, we report U-Th dating results of carbonate formations associated with rock art in three Spanish caves: La Pasiega (Cantabria), Maltravieso (Extremadura), and Doña Trinidad, or Ardales (Andalucía), see Fig. S1 (*20*). Our criteria for sample selection and subsequent sampling strategy strictly followed previously described methods (*14*). The reliability of the U-Th dating results is controlled by quality criteria for the carbonate (*14*) as well as by the collection and analysis of multiple subsamples of a given crust.

La Pasiega is part of the Monte Castillo cave art complex, a World Heritage site that also includes the caves of El Castillo, Las Chimeneas and Las Monedas. Together, these caves show continued human occupation through the last 100,000 years. At La Pasiega, the rock art comprises mainly red and black paintings, including groups of animals, linear signs, claviform signs, dots, and possible anthropomorphs (*21*). Maltravieso was episodically used by hominin groups during the last 180,000 years (*22*); it contains an important set of red hand stencils (~60), which form part of a larger body of art that includes both geometric designs (e.g., dots and triangles) and painted and engraved figures (*23*). Ongoing excavations have shown that Ardales was occupied in the Middle and the Upper Palaeolithic; its walls feature an impressive number (>1000) of paintings and engravings in a vast array of forms, including hand stencils and prints, numerous dots, discs, lines and other geometric shapes, as well as figurative representations of animals, including horse, deer and birds (*24*).

We obtained U-Th ages for 53 samples removed from 25 carbonate formations stratigraphically related to paintings in these caves. Full methods and dataset are presented in (*20*). Here we present and discuss the results most significant for the antiquity of the art.

In La Pasiega C (Fig. S2), a cauliflower type carbonate formation on top of a red scalariform sign (Panel 78 of Hall XI, Fig. 1 and (*20*)) yielded U-Th dates for three subsamples (outer, middle and inner) that increase in age with depth, i.e. towards the pigment layer. They provide a minimum age of 64.8 ka (PAS 34) (Table 1 and (*20*)) for the sign.

In Maltravieso (Fig. S7), we dated samples from five locations on various carbonate formations overlying the same red hand stencil (motif GS3b, Fig. 2 and (*20*)). Carbonate deposits almost completely obscure this hand stencil, making it difficult to see it by naked eye and to record by conventional photography. Fig. 2 therefore also shows a version of the photographic documentation after DStretch (*25*) was applied. For sub samples in all locations, the expected

depth–age consistency was confirmed. The oldest date provides a minimum age of 66.7 ka (MAL 13) (Table 1 and (*20*)) for the hand stencil.

In Ardales (Fig. S9), we dated layers of five carbonate curtains from three areas of the cave (II-A, II-C and III-C) that had been painted red. In three cases, we were able to obtain both maximum and minimum ages by dating samples from immediately underneath the pigment and from carbonate that subsequently formed on top. These age pairs constrain one or more episodes of painting to between 48.7 ka and 45.3 ka (ARD 14 and 15), 45.5 ka and 38.6 ka (ARD 26 and 28) and 63.7 and 32.1 ka (ARD 6 and 8) (Table 1 and (*20*)). A further two samples yielded minimum ages: of 65.5 ka (ARD 13, Fig. 3), demonstrating an earlier episode of painting, and of 45.9 ka (ARD 16), consistent with the other episodes, Fig. S42 *(20)*.

Criteria for reliable minimum (or maximum) ages (*14*) were met by all samples. The oldest minimum ages from the three caves are consistent and, at 64.8 ka or older for each site, significantly pre-date the arrival of modern humans in Europe which has been variously estimated at between 45 and 40 ka (*26, 27*). Our dating results show that cave art was being made at La Pasiega, Maltravieso and Ardales by at least 20,000 years before that. In this age range Iberia was populated by Neanderthals, represented by numerous diagnostic osteological remains, including articulated skeletons (*28, 29*). The implication is, therefore, that the artists involved were Neanderthal.

All examples of early cave art dated so far were created in red pigment, and comprise dots, lines, disks and hand stencils (*30*). This is a restricted and non-figurative set of subjects, and could represent the extension to the external world of marks already created by Neanderthals on their bodies. Whether or not concentrations of colour, dots/disks and linear motifs can be conceived as symbolic, hand stencils (which, unlike positive hand prints, cannot be created by accident) required a light source and previous selection and preparation of the colouring material – evidence of premeditated creation. As a number seem to have been deliberated placed in relation to natural features in caves rather than randomly created on accessible surfaces (*31*), it is difficult to see them as anything but meaningful symbols placed in meaningful places.

This cave painting activity constitutes symbolic behaviour by definition, and one that is deeply rooted. At Ardales, distinct episodes over a period of more than 25,000 years corroborate that we are not dealing with a one-off burst but with a long tradition that may well stretch back to the time of the annular construction found in Bruniquel Cave, France (*32*), dated to 176.5 ± 2.1 ka. Dating results for the excavation site at Cueva de los Aviones (Spain) (*2*), which place

symbolic use of marine shells and mineral pigments by Neanderthals at >120 ka (*33*), further support the antiquity of Neanderthal symbolism.

Cave art like that dated here exists in other caves of western Europe and could potentially be of Neanderthal origin as well. Red-painted draperies are found at Les Merveilles (France; Panel VII) (*34*) and at El Castillo (Spain), while hand stencils and linear symbols are ubiquitous and, when part of complex superimpositions, always form the base of pictorial stratigraphies. We therefore expect that cave art of Neanderthal origin will eventually be revealed in other areas with Neanderthal presence elsewhere in Europe. We also see no reason to exclude that the behaviour will be equally ancient among coeval non-Neanderthal populations of Africa and Asia.

The authorship of the so-called "transitional" techno-complexes of Europe that, like the Châtelperronian, feature abundant pigments and objects of personal ornamentation, has long been the subject of much debate (*35, 36*). Direct or indirect (via acculturation) assignment to modern humans has been based on an "impossible coincidence" argument – the implausibility that Neanderthals would independently evolve the behaviour just at the time when modern humans were already in or at the gates of Europe. By showing that the Châtelperronian is but a late manifestation of a long-term indigenous tradition of Neanderthal symbolic activity, our results bring closure to this debate.

References and Notes

1. C. Henshilwood, F. d´Errico, *Homo symbolicus. The dawn of language, imagination and spirituality*. (John Benjamins Publishing Company, Amsterdam, 2011).
2. J. Zilhão *et al.*, Symbolic use of marine shells and mineral pigments by Iberian Neandertals. *Proceedings of the National Academy of Sciences of the United States of America* **107**, 1023-1028 (2010).
3. M. Peresani, I. Fiore, M. Gala, M. Romandini, A. Tagliacozzo, Late Neandertals and the intentional removal of feathers as evidenced from bird bone taphonomy at Fumane Cave 44 ky B.P., Italy. *Proceedings of the National Academy of Sciences of the United States of America* **108**, 3888-3893 (2011).
4. D. Radovčić, A. O. Sršen, J. Radovčić, D. W. Frayer, Evidence for neandertal jewelry: Modified white-tailed eagle claws at krapina. *PLoS ONE* **10**, (2015).
5. C. S. Henshilwood, F. d'Errico, I. Watts, Engraved ochres from the Middle Stone Age levels at Blombos Cave, South Africa. *J. Hum. Evol.* **57**, 27-47 (2009).
6. C. S. Henshilwood *et al.*, A 100,000-year-old ochre-processing workshop at Blombos Cave, South Africa. *Science* **334**, 219-222 (2011).
7. F. d'Errico, C. Henshilwood, M. Vanhaeren, K. van Niekerk, Nassarius kraussianus shell beads from Blombos Cave: Evidence for symbolic behaviour in the Middle Stone Age. *J. Hum. Evol.* **48**, 3-24 (2005).

8. A. Leroi-Gourhan, B. Delluc, G. Delluc, *Préhistorie de l´art occidental*. (Citadelles & Mazenod, Paris, 1995).
9. P. Pettitt, A. Pike, Dating European Palaeolithic cave art: Progress, prospects, problems. *J. Archaeol. Method Theory* **14**, 27-47 (2007).
10. J. C. Marquet, M. Lorblanchet, A Neanderthal face? The proto-figurine from La Roche-Cotard, Langeais (Indreet-Loire, France). *Antiquity* **77**, 661-670 (2003).
11. J. Rodríguez-Vidal *et al.*, A rock engraving made by Neanderthals in Gibraltar. *Proceedings of the National Academy of Sciences of the United States of America* **111**, 13301-13306 (2014).
12. P. Pettitt, Is this the infancy of art? Or the art of an infant? A possible Neanderthal face from La Roche-Cotard, France. *Before Farming* **2003**, 1-3 (2003).
13. E. Camarós *et al.*, Bears in the scene: Pleistocene complex interactions with implications concerning the study of Neanderthal behavior. *Quat. Int.* **435**, 237-246 (2017).
14. D. L. Hoffmann, A. W. G. Pike, M. García-Diez, P. B. Pettitt, J. Zilhão, Methods for U-series dating of CaCO3 crusts associated with Palaeolithic cave art and application to Iberian sites. *Quat. Geochronol.* **36**, 104-119 (2016).
15. Note: Minimum ages are calculated by subtracting the 95 % uncertainty from the mean; maximum ages are calculated by adding the 95 % uncertainty to the mean.
16. M. Aubert *et al.*, Pleistocene cave art from Sulawesi, Indonesia. *Nature* **514**, 223-227 (2014).
17. A. W. G. Pike *et al.*, U-Series Dating of Paleolithic Art in 11 Caves in Spain. *Science* **336**, 1409-1413 (2012).
18. J. J. Hublin, The modern human colonization of western Eurasia: when and where? *Quat. Sci. Rev.* **118**, 194-210 (2015).
19. J. Zilhão, Chronostratigraphy of the Middle-to-Upper Paleolithic transition in the Iberian Peninsula. *Pyrenae* **37**, 7-84 (2006).
20. Supplementary Materials
21. H. Breuil, H. Obermaier, H. Alcalde del Río, *La Pasiega à Puente Viesgo (Santander, Espagne)*. (Institut de Paléontologie Humaine, Chêne, Mónaco, 1913).
22. N. Barrero *et al.*, in *O Paleolitico, Actas do IV Congreso de Arqueología Peninsular*, N. Bicho, Ed. (Universidade do Algarve: Faro, 2005), pp. 265–284.
23. H. Collado, J. J. García, Handprints in Matravieso Cave (Cáceres, Spain): Typology, Distribution, Techniques and Chronological Context. *IFRAO 2013 Proceedings American Indian Rock Art* **40**, 383-440 (2013).
24. P. Cantalejo *et al.*, *La cueva de Ardales: arte prehistórico y ocupación en el Paleolítico*. (Diputación de Málaga, Málaga, 2006).
25. P. Clogg, M. Díaz-Andreu, B. Larkman, Digital image processing and the recording of rock art. *J. Archaeol. Sci.* **27**, 837-843 (2000).
26. J. Zilhão, F. D'Errico, The chronology and taphonomy of the earliest Aurignacian and its implications for the understanding of Neandertal extinction. *J. World Prehist.* **13**, 1-68 (1999).
27. T. Higham *et al.*, The timing and spatiotemporal patterning of Neanderthal disappearance. *Nature* **512**, 306-309 (2014).
28. M. J. Walker *et al.*, Late Neandertals in Southeastern Iberia: Sima de las Palomas del Cabezo Gordo, Murcia, Spain. *Proceedings of the National Academy of Sciences of the United States of America* **105**, 20631-20636 (2008).
29. R. E. Wood *et al.*, A new date for the neanderthals from el sidrón cave (asturias, northern spain). *Archaeometry* **55**, 148-158 (2013).
30. M. García-Diez *et al.*, The chronology of hand stencils in European Palaeolithic rock art: Implications of new u-series results from el Castillo cave (Cantabria, Spain). *J. Anthropol. Sci.* **93**, 135-152 (2015).

31. P. Pettitt, A. M. Castillejo, P. Arias, R. O. Peredo, R. Harrison, New views on old hands: The context of stencils in El Castillo and la Garma caves (Cantabria, Spain). *Antiquity* **88**, 47-63 (2014).
32. J. Jaubert *et al.*, Early Neanderthal constructions deep in Bruniquel Cave in southwestern France. *Nature* **534**, 111-114 (2016).
33. D. L. Hoffmann, D. E. Angelucci, V. Villaverde, J. Zapata, J. Zilhão, Symbolic Use of Marine Shells and Mineral Pigments by Iberian Neanderthals 115,000 years ago. (submitted).
34. M. Lorblanchet, *Art Pariétal - Grottes ornées du Quercy*. (Edition Rouergue, Rodez, 2010), pp. 446.
35. P. Mellars, Neanderthal symbolism and ornament manufacture: The bursting of a bubble? *Proceedings of the National Academy of Sciences of the United States of America* **107**, 20147-20148 (2010).
36. F. Caron, F. d'Errico, P. Del Moral, F. Santos, J. Zilhão, The reality of neandertal symbolic behavior at the grotte du renne, arcy-sur-cure, france. *PLoS ONE* **6**, (2011).
37. D. L. Hoffmann *et al.*, Procedures for accurate U and Th isotope measurements by high precision MC-ICPMS. *Int. J. Mass Spectrom.* **264**, 97-109 (2007).
38. K. Mathew, P. Mason, A. Voeks, U. Narayanan, Uranium isotope abundance ratios in natural uranium metal certified reference material 112-A. *Int. J. Mass Spectrom.* **315**, 8-14 (2012).
39. S. Richter *et al.*, "REIMEP 18: Inter-laboratory comparison for the measurement of uranium isotopic ratios in nitric acid solution," (Institute for Reference Materials and Measurements, Luxembourg, 2006).
40. S. Richter *et al.*, Re-certification of a series of uranium isotope reference materials: IRMM-183, IRMM-184, IRMM-185, IRMM-186 and IRMM-187. *Int. J. Mass Spectrom.* **247**, 37-39 (2005).
41. K. W. W. Sims *et al.*, An inter-laboratory assessment of the thorium isotopic composition of synthetic and rock reference materials. *Geostand. Geoanal. Res.* **32**, 65-91 (2008).
42. A. H. Jaffey, K. F. Flynn, L. E. Glendenin, W. C. Bentley, A. M. Essling, Precision Measurement of Half-Lives and Specific Activities of U-235 and U-238. *Phys. Rev. C* **4**, 1889-& (1971).
43. H. Cheng *et al.*, The half-lives of uranium-234 and thorium-230. *Chem. Geol.* **169**, 17-33 (2000).
44. N. E. Holden, Total Half-Lives for Selected Nuclides. *Pure Appl. Chem.* **62**, 941-958 (1990).
45. S. J. Goldstein, M. T. Murrell, D. R. Janecky, Th and U isotopic systematics of basalts from the Juan de Fuca and Gorda Ridges by mass spectrometry. *Earth Planet. Sci. Lett.* **96**, 134-146 (1989).
46. J. Prytulak, T. Elliott, D. L. Hoffmann, C. D. Coath, Assessment of USGS BCR-2 as a reference material for silicate rock U-Pa disequilibrium measurements. *Geostand. Geoanal. Res.* **32**, 55-63 (2008).
47. E. P. Horwitz *et al.*, Separation and preconcentration of uranium from acidic media by extraction chromatography. *Anal. Chim. Acta* **266**, 25-37 (1992).
48. D. L. Hoffmann *et al.*, Characterisation of secondary electron multiplier nonlinearity using MC-ICPMS. *Int. J. Mass Spectrom.* **244**, 97-108 (2005).
49. M. García-Diez, Palaeolithic caves of northern Spain: World Heritage Site. *Rock Art Res.* **26**, 99-101 (2009).
50. A. W. G. Pike, D. L. Hoffmann, P. B. Pettitt, M. García-Diez, J. Zilhão, Dating Palaeolithic cave art: Why U–Th is the way to go. *Quat. Int.* **432**, 41-49 (2017).
51. K. H. Wedepohl, The Composition of the Continental-Crust. *Geochim. Cosmochim. Acta* **59**, 1217-1232 (1995).

Acknowledgments: This research was financially supported by the Natural Environment Research Council (UK) (Grant NE/K015184/1), the National Geographic Society (USA) (Grant EC0603-12) and the Max Planck Society (Germany) and a Royal Society Wolfson Research Merit Award (to AWGP). The work of MGD was supported by the Research Group IT622-13 of the Basque Government. We thank the governments of Andalucía, Cantabria and Extremadura for sampling permissions. We are grateful for fieldwork support by Juan Carlos Aguilar, Mireille Batut, José Ramón Bello, Daniel Garrido, Raúl Gutiérrez and Carola Hoffmann. The data described are presented in the supplementary materials.

Figure legends

Fig. 1: Red scalariform sign, Panel 78 ('La Trampa' (*21*) in Hall XI, La Pasiega C. The insert shows the crust sampled and analyzed for a minimum age (64.8 ka) constraining the age of the red line. See (*20*) for details.

Fig. 2: Hand stencil GS3b in Maltravieso cave (minimum age 66.7 ka). The upper picture shows the original photo, the lower image is the same picture after application of DStretch (*25*) (Correlation LRE 15%, auto contrast) to enhance colour contrast. The inset shows where the overlying carbonate was sampled for MAL 13. See (*20*) for details

Fig. 3: Speleothem curtain 8 in section II-A-3 in Ardales cave with red pigment, painted prior to at least 65.5 ka ago. Left: the series of curtains with red paint on top, partly covered with later speleothem growth. The white rectangle denotes the area shown on the right. Right: Detail of curtain 8, the black rectangle denotes where carbonate, overlying the red paint, was sampled for ARD 13. See (*20*) for details.

Supplementary materials

Materials and methods

1. Analytical methods: U-series dating of carbonate crusts
2. Cave sites and cave art
3. Carbonate samples

Supplementary text

1. U-series results

Figures S1 - S42

Table S1 - S4

References (37-51)

Fig. 1

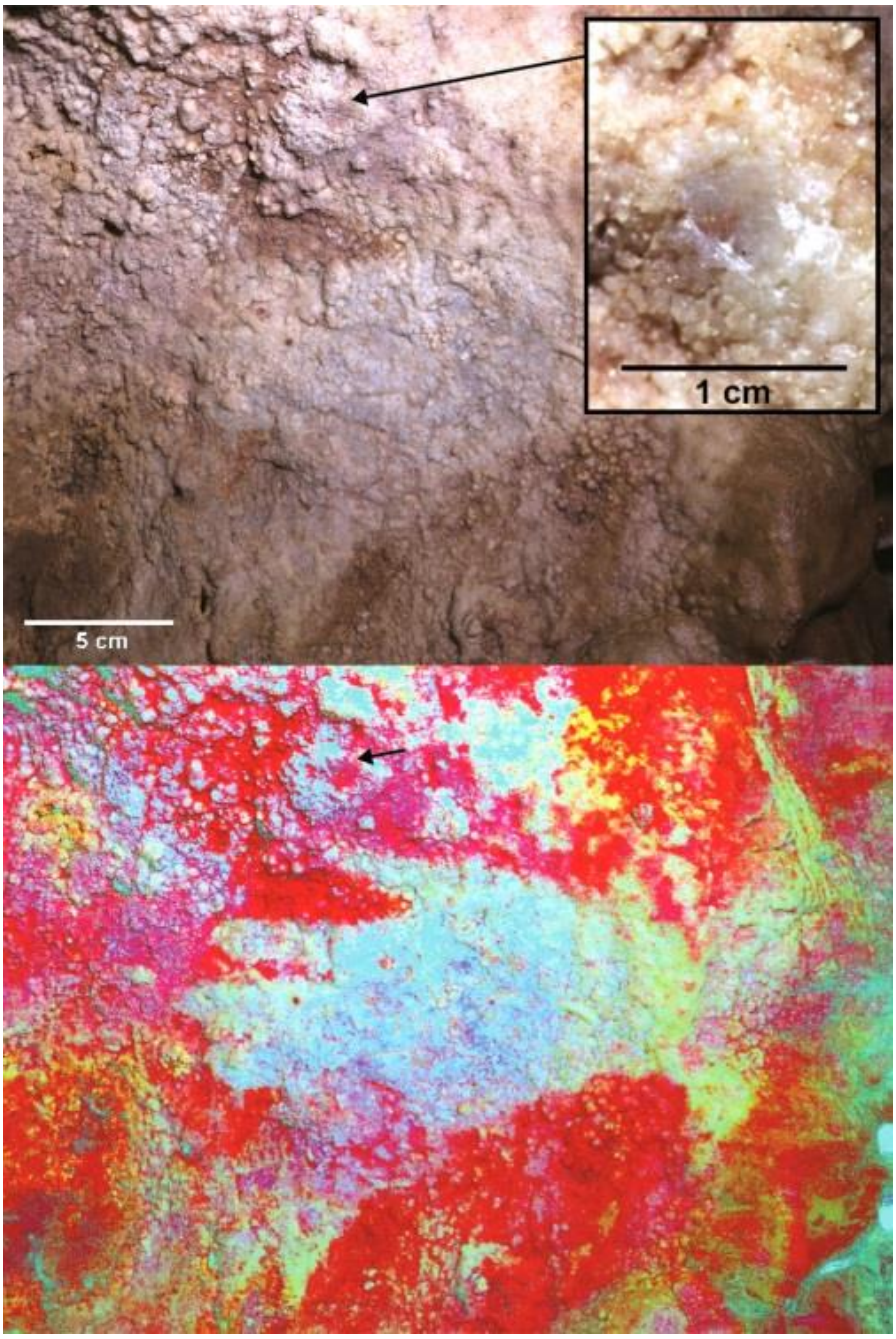

Fig. 2

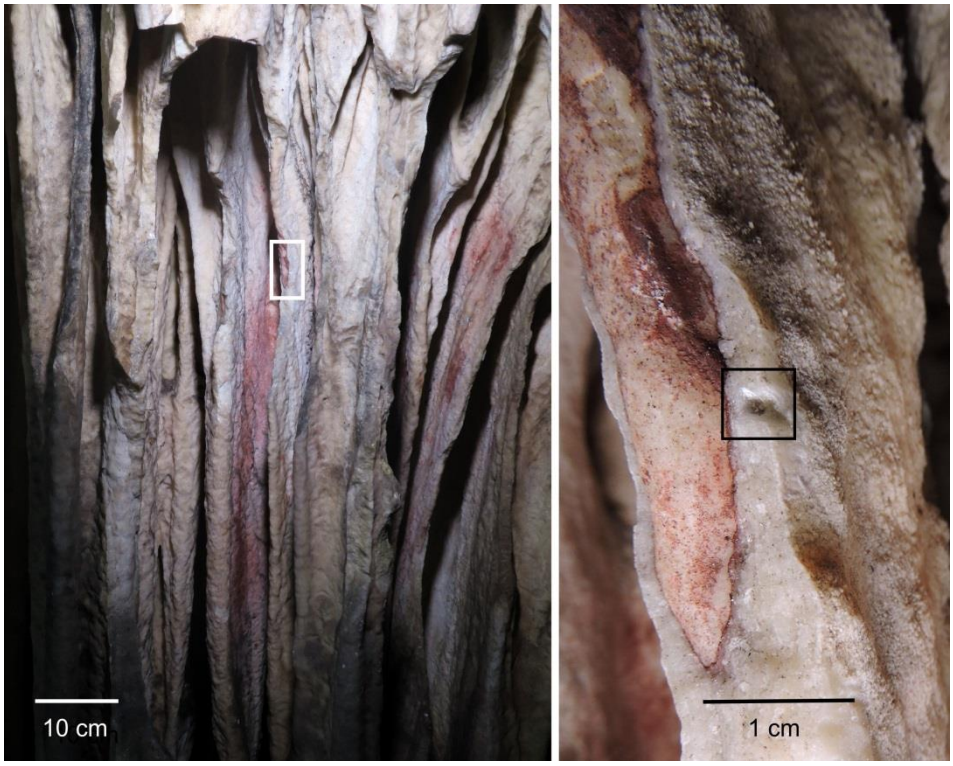

Fig. 3

Table 1.

U-series results of samples discussed in the text. More details and additional results can be found in Table S4 (*20*).

Spl ID	***Site and description***	**^{238}U** [ng/g]	**^{230}Th/^{232}Th**	**^{230}Th/^{238}U** *uncorrected*	**^{234}U/^{238}U** *uncorrected*	**Age** *uncorrected* [ka]	**Age** *corrected* [ka]
PAS 34a	Pasiega C, No. 78, cauliflower type carbonate on top of red line of scalariform motif, minimum age	289.29 ± 9.06	32.82 ± 0.21	1.5149 ± 0.0106	3.7694 ± 0.0082	52.52 ± 0.47	51.56 ± 1.09
PAS 34b	as above	215.56 ± 7.43	28.28 ± 0.19	1.5453 ± 0.0121	3.6744 ± 0.0094	55.53 ± 0.56	54.36 ± 1.39
PAS 34c	as above	178.31 ± 8.31	7.25 ± 0.07	2.0348 ± 0.0213	3.4591 ± 0.0092	85.79 ± 1.28	79.66 ± 14.90
MAL 13 surface cleaning fraction	Maltravieso, cauliflower type carbonate layer overlying hand stencil GS3b, minimum age	117.2 ± 1.99	12.47 ± 0.16	0.4639 ± 0.0068	1.1872 ± 0.0328	53.3185 + 2.30 - 2.13	41.68 + 2.44 - 2.29
MAL 13A	as above	142.69 ± 3.39	37.50 ± 0.57	0.6067 ± 0.0123	1.2024 ± 0.0305	74.8553 + 3.78 - 3.41	70.08 + 3.82 - 3.37
ARD 06	Ardales, red paint on curtain formation, II-C-8, carbonate from underlying curtain, maximum age	511.42 ± 6.38	34.95 ± 0.14	0.4661 ± 0.0021	1.0459 ± 0.0021	64.09 ± 0.44	62.97 ± 0.69
ARD 08	Ardales, red paint on curtain formation, II-C-8, carbonate from overlying curtain, minimum age	297.21 ± 2.89	145.58 ± 1.06	0.2703 ± 0.0018	1.0477 ± 0.0024	32.51 ± 0.26	32.35 ± 0.27
ARD 13A	Ardales, red paint on curtain formation, II-A-3 curtain 8, minimum age	1229.61 ± 25.84	152.83 ± 1.14	0.3661 ± 0.0033	1.0385 ± 0.0033	47.3312 + 0.57 - 0.56	47.13 + 0.56 - 0.57
ARD 13B	as above	331.54 ± 13.53	42.59 ± 0.58	0.4878 ± 0.0073	1.0369 ± 0.0234	69.093 + 2.93 - 2.62	68.13 + 2.96 - 2.62

ARD 14A	Ardales, red paint on curtain formation, II-A-3 curtain 6, carbonate from underlying curtain, maximum age	684.76 ± 13.29	395.03 ± 4.91	0.3683 ± 0.0063	1.0379 ± 0.0029	47.72 + 1.05 - 1.02	47.64 + 1.07 - 1.03
ARD 15A	Ardales, red paint on curtain formation, II-A-3 curtain 6, carbonate from overlying curtain, minimum age	1696.03 ± 53.88	337.14 ± 3.63	0.3584 ± 0.0050	1.0374 ± 0.0025	46.15 + 0.81 - 0.82	46.06 + 0.81 - 0.77
ARD 15B	as above	667.98 ± 37.85	152.07 ± 3.27	0.3467 ± 0.0110	1.0347 ± 0.0061	44.45 + 1.79 - 1.82	44.25 + 1.78 - 1.77
ARD 16A	Ardales, red paint on curtain formation, II-A-3 curtain 5, carbonate from overlying curtain, minimum age	313.84 ± 5.88	58.92 ± 0.74	0.3317 ± 0.0044	1.0323 ± 0.0051	42.23 + 0.74 - 0.72	41.75 ± 0.77
ARD 16B	as above	250.2 ± 4.29	84.25 ± 0.84	0.3628 ± 0.0050	1.0314 ± 0.0051	47.23 + 0.85 - 0.83	46.86 + 0.85 - 0.92
ARD 16C	as above	227.59 ± 28.55	56.70 ± 2.84	0.3690 ± 0.0213	1.0227 ± 0.0342	48.79 + 4.26 - 4.00	48.23 + 4.43 - 4.10
ARD 26A	Ardales, red paint visible as a line on cross section of a broken curtain, between III-C-3 and III-C-2, carbonate from overlying curtain, minimum age	564.64 ± 13.56	1004.53 ± 20.81	0.3243 ± 0.0099	1.0502 ± 0.0203	40.20 + 1.84 - 1.69	40.17 + 1.73 - 1.77
ARD 26B	as above	532.37 ± 14.02	985.93 ± 24.33	0.3258 ± 0.0112	1.0496 ± 0.0113	40.45 + 1.82 - 1.70	40.42 + 1.79 - 1.78
ARD 28A	Ardales, red paint visible as a line on cross section of a broken curtain, between III-C-3 and III-C-2, carbonate from underlying curtain, maximum age	520.54 ± 8.11	4626.61 ± 188.57	0.3379 ± 0.0192	1.0458 ± 0.0124	42.48 + 3.09 - 2.91	42.47 + 3.07 - 2.97

All ratios are activity ratios. Analytical errors are at 95 % confidence level.

Supplementary Materials for

U-Th dating of carbonate crusts reveals Neanderthal origin of Iberian cave art

D. L. Hoffmann, C. D. Standish, M. García-Diez, P. B. Pettitt, J. A. Milton, J. Zilhão, J. Alcolea, P. Cantalejo-Duarte, H. Collado, R. de Balbín, M. Lorblanchet, J. Ramos-Muñoz, G.-Ch. Weniger, A. W. G. Pike

This PDF file includes:

Materials and Methods

1. Analytical methods: U-series dating of carbonate crusts

Two U-series laboratories are involved in this study, one housed at the Department of Human Evolution, Max Planck Institute for Evolutionary Anthropology, Leipzig (Germany) and one housed at the Ocean and Earth Science analytical geochemistry facilities, University of Southampton (UK). While both laboratories have similar setups, generally following protocols outlined in (*37*) and (*14*), we report in detail procedures for sample preparation and mass spectrometry for both laboratories.

1.1 U-series methods at the U-series laboratory of the Max Planck Institute for Evolutionary Anthropology (MPI EVA), Leipzig

Samples taken from carbonate crusts associated with cave art are typically collected in pre-cleaned 15 ml plastic tubes. Before further chemical separation and purification, the samples are inspected for detrital particles. In cases where such particles are found, they are removed from the sample powders before they are transferred into Savillex PFA containers as described in detail in (*14*). Separation and purification of U and Th from the sample matrix follows protocols also outlined in (*14*). In brief, the samples are dissolved by adding sufficient 7 M HNO_3, a mixed, accurately calibrated ^{229}Th-^{236}U spike is added and the solution refluxed for equilibration. The spike was gravimetrically prepared from a pure ^{229}Th solution, calibrated against NIST SRM 3159, and IRMM 3600. The mixed spike was then further calibrated following procedures outlined in (*37*). A double resin isotope dilution procedure is used to separate U and Th and then purify each fraction. BioRad AG 1x8 is used to separate U and Th followed by a first purification of the Th fraction also using AG 1x8. Final purification of U and Th fractions is done using Eichrom UTEVA resin. The final U and Th fractions are dissolved in 0.5 M HCl, U and Th isotope compositions of the solutions are separately measured by multi-collector (MC) inductively-coupled plasma mass spectrometry (ICPMS) following (*37*). Procedural chemistry blank values are typically less than 1 pg ^{238}U, 1 fg ^{235}U, 0.1 fg ^{234}U, 1 pg ^{232}Th and 0.1 fg ^{230}Th, respectively.

Mass spectrometry analyses are done with a ThermoFinnigan Neptune MC-ICPMS. The Neptune is equipped with the Neptune plus interface, an energy filter (RPQ) for small ion beams measured on the central ion counter, which is a MasCom SEM. For sample introduction a setup including a Cetac Aridus II with Quickwash and a Savillex PFA nebuliser tip with 35 µl/min uptake rate is used.

A sample - standard bracketing protocol is used for U isotope ratio measurements. U samples are analysed vs. a NBL-112a solution (*37*) employing the certified isotope ratio values from (*38*) with $^{234}U/^{238}U = (5.2841 \pm 0.0082)\cdot10^{-5}$ and $^{235}U/^{238}U = (7.2543 \pm 0.0040)\cdot10^{-3}$. At least two additional U isotope standard solutions are routinely measured along with samples, run with identical setup and similar intensities as sample solutions. These standards include the REIMEP 18 solutions A and B (*39*), the certified reference solution IRMM 183 (*40*) and a purified U fraction of the uraninite solution URAN 84.5 (*37*). The URAN 84.5 U solution has a natural secular equilibrium U isotope composition, Reimep 18 A has an isotopic composition similar to natural U but this standard contains a small amount of ^{236}U. Reimep 18 B and IRMM 183 have $^{236}U/^{238}U$ ratios comparable to spiked samples and non-natural $^{235}U/^{238}U$. This suite of standards is representative of typical U solutions analysed for isotopic compositions. For routine analyses we obtain the isotopic ratios presented in Table S1.

A sample - standard bracketing protocol is also used for Th isotope ratio measurements. However, there is no certified ^{229}Th-^{230}Th-^{232}Th isotope solution available. Hoffmann et al. (2007) (*37*) prepared and calibrated an in-house Th standard (TEDDi), but only small quantities of this solution are left, so it is no longer used as bracketing standard for Th isotope analyses. Instead, a new suite of Th standard solutions has been prepared, one solution (TEDDii) is the replacement solution for TEDDi with similar isotopic composition. This solution is now routinely used as bracketing standard and TEDDi serves as standard which is run as a sample to check accuracy and reproducibility. Two additional Th solutions were prepared, one with $^{230}Th/^{232}Th$ around 0.06 (Thoca), one with $^{230}Th/^{232}Th$ of $1.14\cdot10^{-5}$ (Thosi). Thoca and TEDDii were gravimetrically prepared using a calibrated in-house ^{229}Th spike, the IRMM 61 ^{230}Th spike and NIST SRM 3159 ^{232}Th standard. Thosi was gravimetrically prepared adding a known quantity of the calibrated ^{229}Th spike to a (concentration-) calibrated IRMM 35 solution with a consensus value for $^{230}Th/^{232}Th$ ratio (*41*). All solutions, especially the $^{230}Th/^{229}Th$ ratios, were then additionally calibrated by MC-TIMS and MC-ICPMS as outlined in (*37*). This suite of standards is representative of typical Th solutions analysed for isotopic compositions. During a sequence, we always measure TEDDi and one or two other Th standards, depending on the isotopic range of the measured samples, which is checked by intensity screening prior to analyses. For routine analyses we obtain the isotopic ratios presented in Table S2.

U-Th ratios are calculated from the measured isotopic compositions of the spiked U and Th fractions of a sample using the known $^{229}Th/^{236}U$ ratio of the spike solution. The following decay constants are then used to calculate activity ratios: $\lambda_{238} = (1.55125 \pm 0.0017)\cdot10^{-10}$ a^{-1} (*42*), $\lambda_{234} = (2.826 \pm 0.0056)\cdot10^{-6}$ a^{-1} (*43*), $\lambda_{232} = (4.95 \pm 0.035)\cdot10^{-11}$ a^{-1} (*44*),

λ_{230} = (9.1577 ± 0.028)·10^{-6} a^{-1} (*43*). We routinely prepare a fraction of the URAN 84.5 as part of a set of samples. 34 individually prepared samples of this uraninite solution give activity ratios of $^{234}U/^{238}U$ = 0.9995 ± 0.0005 and $^{230}Th/^{238}U$ = 1.0021 ± 0.0008. We also analysed a sample of the silicate secular equilibrium sample TML (*45*) which yielded $^{234}U/^{238}U$ of 1.0003 ± 0.0015 and $^{230}Th/^{238}U$ of 0.9995 ± 0.0027. For the basaltic reference material USGS BCR-2, analysis of a sample yielded $^{234}U/^{238}U$ of 1.0028 ± 0.0015 and $^{230}Th/^{238}U$ of 1.0058 ± 0.0033, which confirms previously found elevated $^{230}Th/^{238}U$ and $^{234}U/^{238}U$ activity ratios (*37, 46*). U-Th ages are calculated iteratively from the activity ratios and using above decay constants. Uncertainties are calculated using a Monte-Carlo approach (*37*), all uncertainties of the Leipzig laboratory quoted in this study are at 95 % (2σ) confidence level. Minimum ages are calculated as the mean minus 2σ and maximum ages as the mean plus 2σ.

1.2 U-series methods at the Ocean and Earth Science analytical geochemistry facilities, University of Southampton

Carbonate samples, typically between 1 mg and 50 mg in mass and collected in pre-cleaned 15 ml plastic tubes, are first inspected under a low power microscope and detrital particles removed where possible. The samples are then weighed into pre-cleaned Savillex PFA vials, 1.5 ml of 18.2 MΩ·cm (ultrapure) water added, and the samples are dissolved by stepwise addition of concentrated (~15.5 N) HNO_3. A mixed $^{229}Th/^{236}U$ spike (*37*) is added and left to equilibrate for a few hours, after which the sample solutions are evaporated to dryness then re-dissolved in 0.5 ml concentrated HNO_3 and 0.5 ml H_2O_2 and refluxed at 150°C. Finally, the samples are evaporated to dryness and re-dissolved in 6 ml 3 N HNO_3 ready for the ion exchange columns.

Ion exchange chromatography for the separation of U and Th from the sample matrix employ 0.6 ml columns and 100 – 150 μm UTEVA Spec (Eichrom) resin (*47*). After loading into the columns, the resin is cleaned by elution of 4 ml 0.05 N HCl, 5 ml 3 N HCl, then 4 ml ultrapure water. The resin is conditioned with 7 ml 3 N HNO_3 before the samples are loaded in 6 ml 3 N HNO_3. Matrix is eluted in 9 ml 3 N HNO_3, then Th is eluted in 3 ml 3 N HCl followed by U in 8 ml 0.05 N HCl. The Th and U fractions are evaporated to dryness then re-dissolved in 0.5 ml concentrated HNO_3 and 0.5 ml H_2O_2 and refluxed at 150°C before being evaporated to dryness and re-dissolved in 1.8 ml 0.6 N HCl for analysis by mass spectrometer. Procedural chemistry blank values are always less than 0.01 ng ^{238}U, 0.1 pg ^{235}U, 0.01 pg ^{234}U, 0.01 ng ^{232}Th and 1 fg ^{230}Th, respectively.

Sediment samples (~200 mg) are first dissolved following the procedure detailed above. The soluble and insoluble fractions are then separated by centrifuge. The soluble fractions are

spiked with the mixed $^{229}Th/^{236}U$ spike, refluxed for equilibration, then evaporated to dryness before being dissolved in 6 ml 3 N HNO_3 ready for ion exchange chromatography. The insoluble fractions are weighed into pre-cleaned Savillex PFA vials before being dissolved in 1 ml 7 N HNO_3 and 0.5 ml concentrated HF on a hotplate then evaporated to dryness. They are then dissolved in 2 ml 6 N HCl and refluxed before being evaporated to dryness and dissolved in 1 ml 7 N HNO_3 and refluxed. Finally, the samples are spiked with the mixed $^{229}Th/^{236}U$ spike, refluxed for equilibration, then evaporated to dryness and dissolved in 6 ml 3 N HNO_3 ready for the ion exchange chromatography. Ion exchange chromatography follows the same procedure outlined above. The isotopic composition of the total sediment (i.e. combined soluble and insoluble) is calculated using the isotopic composition and mass of both fractions.

U and Th isotope measurements are undertaken using a Thermo Scientific Neptune Plus MC-ICPMS equipped with an energy filter (RPQ) on the central ion counter and housed at the Ocean and Earth Science analytical geochemistry facilities at the University of Southampton. Sample introduction employs a Cetac Aridus II and 75 or 100 µl/min Savillex C-flow PFA nebulisers with typical uptake rates of ~80 µl/min. Analytical procedures follow those outlined in (*37*). The secondary electron multiplier was shown to have a linear response so a correction for nonlinearity (*48*) is not necessary. For Th analyses the H1 and H2 Faraday cup amplifiers are connected to 10^{12} Ω resistors. Instrumental biases (e.g. mass fractionation) are corrected by sample - standard bracketing procedures; CRM-145 is used for U isotope measurements and the Bristol/Leipzig in-house ^{229}Th-^{230}Th-^{232}Th standard solution TEDDii (further details in section 1.1) is used for Th isotope measurements.

For the calculation of activity ratios we use the following decay constants: $\lambda_{230} = (9.1577 \pm 0.028)\cdot10^{-6}$ a^{-1} (*43*), $\lambda_{232} = (4.94752 \pm 0.035)\cdot10^{-11}$ a^{-1} (*44*), $\lambda_{234} = (2.826 \pm 0.0056)\cdot10^{-6}$ a^{-1} (*43*), and $\lambda_{238} = (1.55125 \pm 0.0017)\cdot10^{-10}$ a^{-1} (*42*). U-Th ages are calculated iteratively from the activity ratios and using the above half-lives. Uncertainties, including those for blank correction, are fully propagated, are quoted at 95 % confidence level, and are calculated using a Monte-Carlo approach (*37*). Minimum ages are calculated as the mean minus 2σ and maximum ages as the mean plus 2σ. A secular equilibrium standard, uraninite URAN 84.5, was repeatedly analysed for the duration of the period of data collection as a demonstration of both accuracy and external reproducibility. A single aliquot of the uraninite solution was spiked and prepared following the methods detailed above before being analysed multiple times with every sequence of unknown samples. Our analyses gave the following activity ratios: $(^{230}Th/^{238}U) = 1.0026 \pm 0.0007$ and $(^{234}U/^{238}U) = 1.0001 \pm 0.0002$ (errors are given as 2σ standard errors of the mean, n = 50 over a ~1.5 year period). This is

comparable to the values published for the same solution (*37*). Analyses of a dissolved pristine speleothem sample, which serves as an internal standard solution, were also performed as a further demonstration of external reproducibility. Each analysis of a fraction of the solution equates to a sample size of 18 – 37 mg carbonate. Each was spiked and processed through ion exchange chromatography independently, and was analysed at comparable intensities to other, unknown, carbonate samples. Analyses gave the following: ($^{230}Th/^{238}U$) = 0.4335 ± 0.0082, ($^{234}U/^{238}U$) = 1.0462 ± 0.0053, age = 58.15 ± 1.45 ka (errors are given as 2σ standard deviations of the mean, n = 14 over a ~1 year period).

2. Cave sites and cave art

2.1 Locations of cave sites

Our study includes cave art from three different sites in Spain. They are located in Puente Viesgo, Cantabria (La Pasiega cave), Cáceres, Extremadura (Maltravieso cave) and Ardales, Andalusia (Doña Trinidad, or Ardales cave). Fig. S1 shows the locations of the three sites in northern, central-western and southern Spain.

2.2 La Pasiega C

La Pasiega is one of five caves in the Monte Castillo, located in Puente Viesgo (Cantabria, Spain) in northern Spain (Fig. S1). Five of the caves (El Castillo, Las Monedas, La Pasiega, Las Chimeneas and La Cantera) contain Palaeolithic cave art and, excluding La Cantera, are included in the UNESCO World Heritage site 'Cave of Altamira and Paleolithic Cave Art of Northern Spain' (*49*). La Pasiega has three main galleries (A, B and C, Fig. S2). The art mainly consists of red and black paintings - including groups of animals, linear signs, claviform signs, dots and possible anthropomorphs – but there are also engravings, of animals and of linear forms.

Pike et al. (*17*, *50*) published 18 results on carbonate crusts collected in La Pasiega. Nine of these samples were from gallery C, which we revisited in 2013 and where we collected twelve new samples (PAS 28 to PAS 39). Details and results of the first five of them (PAS 28 - PAS 32) have already been presented in (*14*), including demonstration of reliability of our methods in general and robustness of the results for this gallery in particular. Here we focus on sample PAS 34, sampled on Panel 78, but also give details for the other samples (PAS 33 and PAS 35 - PAS 39).

On top of a rectangular motif in Panel 78 (*21*) (Figs. S3 and S4), we sampled three carbonate crusts. Breuil et al. named the motif 'La Trampa' (The Trap), but it is better described as a scalariform associated with incomplete zoomorphs, red dots and a symbol (Fig. S4). A

parietal stratigraphy - the zoomorphs earlier than the red lines - is described by (*21*), but we could not observe any superimposition of lines. Samples PAS 33, PAS 34 and PAS 38 (Fig. S5) were taken from crusts found on top of red pigment of different parts of this Panel. PAS 33 and PAS 34 are associated with the red lines forming a rectangular shape, PAS 38 is associated with a series of red dots above the rectangular drawing. A sample previously collected from a carbonate crust associated with one of these dots (PAS 3 / BIG-O-99 (*17*)) had returned an age of 12.6 ± 0.1 ka.

Sample PAS 35 (Fig. S6a) was collected from a crust that formed on top of a red deer located in Panel 78 (*21*), left to the series of red dots above the scalariform motif (Fig. S3). Sample PAS 36 (Fig. S6b) was collected from a carbonate formation on top of a red zoomorph, identified as a hind by Breuil et al. (Panel 82, (*21*)). Sample PAS 37 (Fig. S6c) was collected from a crust which formed on top of a red tectiform ('hut' shape) (Panel 76, (*21*). Sample PAS 39 (Fig. S6d) was collected from a crust associated with another red tectiform (Panel 72; (*21*)). These samples were all collected in the same sector of the cave, Breuil et al.'s (*21*) Hall XI.

2.3 Maltravieso

The Cueva de Maltravieso is located in the city of Cáceres, Extremadura, in central-western Spain (Fig. S1). Re-discovered in 1951 during quarrying operations, it was found to contain a rich set of Palaeolithic parietal art. Animal paintings and engravings, including horses, bulls and ibex, are found alongside dots, triangles, red-painted speleothems, red discs and lines and an impressive collection of over 60 red hand stencils. For this study we collected samples from a carbonate crust overlying hand stencil GS3b in the cave's Galería de la Serpiente (Fig. S7). The stencil is covered by thick carbonate formations rendering it difficult to see today. DStretch software is therefore used to enhance digital photography and help view this panel (Fig. S8).

2.4 Ardales

The Cueva de Ardales, Andalusia, is located in southern Spain (Fig. S1). Fig. S9 shows a map of the site. It is rich in speleothem formation including numerous curtain-type formations. It also contains over 1000 artistic images (*24*). These include paintings and engravings, both figurative and non-figurative, such as horse, deer, birds, dots, discs, lines and hand stencils. Zones with red pigment with no defined form or shape can be found on many of the curtain formations in Ardales. In many cases the speleothem growth continued after a surface had been painted on. Therefore the red pigment, typically used for paintings in the cave, was included inside the speleothem formation as a layer. In other cases, the pigment was only partly

overgrown by speleothem. This process is best observed in the several instances where curtain formations have been broken, possibly due to seismic activities or human impact in the past. In some cases, the breakage has exposed cross sections of speleothems where red paint appears as an interstratified layer. Fig. S10 shows a prominent example of such a case (Panel II-C-8). On the right, above the break, a red painted area without overgrowth is apparent. To the left, the red pigment is covered by a thick carbonate overgrowth, and the red layer extends to join the painted surface to the right. The previous surface of the red painted area underneath the speleothem layer can be seen as a red line inside the speleothem. Similar configurations were found on many curtain formations in Ardales (Figs. S11, S12, S13). In some cases the painting was completely included into the speleothem and only appears as a red line in cross-section where breakage has occurred (Fig. S14) though in most cases the pigment is only partially obscured by carbonate growth. We sampled carbonates from curtain or stalactite formations with red painted areas in Panels II-C-8, II-A-3 and between III-C-2 and III-C-3 (Fig. S9).

3. Carbonate samples

Carbonate deposits with a direct association to pigment, i.e. formations either directly overlying or underlying art, were selected for sampling. Samples were taken using either a hand-drill and carbide drill bits or by scraping with a scalpel, with carbonate collected directly into pre-cleaned plastic sample tubes. The sample locations were first documented and mechanically cleaned to remove surface contamination or altered material. Carbonate was then collected in spits to provide a sequence of sub-samples for each sampling location, offering a test for the internal consistency of each dated formation.

The material removed during the surface cleaning of the crusts (the 'cleaning' sub-sample) was sometimes collected. This fraction was usually not taken for the purpose of dating. However, some were analysed when only one further sub-sample could be collected from a sample location. Further details of our sampling procedures are presented in (*14*).

3.1 La Pasiega C

3.1.1 Sampling on Panel 78

All samples were removed by scraping with a scalpel and the carbonate collected directly into the pre-cleaned plastic sample tubes. Prior to sample collection, the surface of the carbonate crust was first cleaned to minimise impact of surface contamination/alteration, but the crusts were thick enough so the cleaning fractions were not collected. PAS 34 was collected from a small cauliflower type carbonate crust, which formed in the lower section on the left vertical

red line which is part of the scalariform painting. The front part of an animal is painted right to the red line. Appearance of the carbonate crust was slightly greyish, but after removal of the surface layer, white, crystalline carbonate was exposed. The crust was a few mm thick, so three subsequent sub-samples with masses between 4 – 6 mg could be scraped off. The crust started to fragment when the sub-sample PAS 34c was scraped, so sampling was stopped to avoid any damage to the painting. Pigment was clearly revealed underlying the carbonate crust (Fig. S15).

3.2 Maltravieso

Two sampling trips were made to la Cueva de Maltravieso in 2014 and 2016. Here we present U-Th dating of carbonates associated with a newly discovered red hand stencil (Panel GS3b) located in la Galería de la Serpiente. An overhang of the cave wall creates a small cove extending from the current cave floor to approximately 1 m in height, and the stencil is on the 'ceiling' of this cove. All samples were removed by scraping with a scalpel, with carbonate collected directly into pre-cleaned plastic sample tubes. Prior to sample collection, the sample locations were first documented and cleaned to remove surface contamination/alteration.

3.2.1 Sampling hand stencil GS3b

Five sampling locations, associated with a hand stencil near Panel 3, now termed Panel 3b, were targeted: MAL 13, MAL 14, MAL 15, MAL 17 and MAL 19 (Fig. S16). All samples are in association with pigment adjacent to the thumb of the stencil. Before sampling, pigment was clearly visible in the valleys and cracks between carbonate growths.

MAL 13 (Figs. S16, S17, S18) consists of two sequential sub-samples (including the surface cleaning fraction) of a crystalline cauliflower formation. MAL 14 (Figs. S16, S19) is located approximately 30 mm 'above' MAL 13, and consists of three sequential sub-samples of a large cauliflower formation (Figs. S18 and S19). MAL 15 (Figs. S16, S20, S21) is located immediately next to MAL 14. It consists of six sequential sub-samples scraped from a solid, agglomerated cauliflower formation. The sampling area had to be widened during collection of sub-samples B and C, therefore mixing with younger carbonate may have occurred. During collection of sub-sample E a new, paler, carbonate layer appeared. MAL 17 (Figs. S22 and S23) is located approximately 100 mm nearer the wrist of the stencil than the previous samples (Fig. S16). It consists of four sub-samples taken from a cream-coloured, crystalline, cauliflower formation. A similar stratigraphy to MAL 15 was noticed, with a paler, whiter, lower layer underlying the creamy-coloured surface carbonate. This paler layer became visible during the collection of sub-sample B, and was directly sampled by sub-samples C and D. The sample area was enlarged during collection of sub-sample B, which may affect the stratigraphy of the sample sequence. MAL 19 (Figs. S16, S24, S25) is located approximately 30 mm towards the

stencil's thumb from MAL 13. It consists of two sub-samples (including the surface cleaning fraction) sampled from a pale/translucent cauliflower formation.

3.2.3 Maltravieso Sediment Samples

Three samples of cave sediment (MAL Sed 1 – 3) were collected from the cave floor near to Panels III and IV in the Sala de las Pinturas. These were taken to provide a proxy for the composition of detrital thorium incorporated within the carbonate samples.

3.2.4 Maltravieso Stalagmitic Column

A small ~30 mm section of a stalagmitic formation, that was probably formerly part of a column broken in antiquity, was removed using a chisel from a platform above Panel IV in the Sala de las Pinturas (MAL 24). It was collected to provide a series of stratigraphically ordered samples that could be dated to assess validity of our detrital thorium corrections. For this purpose, six carbonate layers were sampled in a laboratory environment using a hand-drill to obtain powder samples for dating.

3.3. Ardales

La Cueva de Ardales was sampled in September 2016. Here we present U-Th dating of carbonates associated with red pigment from three panels: II-A-3, an area between Panels III-C-2 and III-C-3 and Panel II-C-8. Samples were taken using either a hand-drill and carbide drill bits or by scraping with a scalpel, with carbonate collected directly into pre-cleaned plastic sample tubes. Prior to sample collection, the sample locations were first cleaned to remove any surface contamination/alteration.

3.3.1 Sampling on Panel II-A-3

Panel II-A-3 consists of a series of painted curtain formations which have formed radiating from a large free standing stalagmitic boss (i.e. not connected to the cave wall). These curtains have fractured at some point during antiquity revealing pigment in section, giving the opportunity to sample carbonate that provides both minimum and maximum dates for the application of the pigment. Samples ARD 12 – 16 relate to this formation.

Samples ARD 12 and ARD 13 are taken from carbonate overlying pigment applied to the right side of curtain 8 (Figs. S26 and S28). They were both collected by drilling into the broken edge of the curtain, and both represent minimum ages for the pigment.

ARD 12 (Figs. S26 and S27) consists of four sequential sub-samples, however it was noted whilst sampling that this series of samples is not strictly in stratigraphic order and sub-sample A (Fig. S26c) was collected from a much larger area than sub-samples B – D (Figs. S26d - f).

This is seen most clearly on Fig. S27 as a wider sampling slot towards the surface. The large sample size of sub-sample A allowed a repeat analysis to be performed as a demonstration of reproducibility. ARD 13 (Figs. S28 and S29) is located about 40 mm above ARD 12 and consists of two sequential sub-samples.

Samples ARD 14 and ARD 15 date pigment applied to the left side of curtain 6 (Figs. S30, S31, S32), and both were collected using a hand-drill. A historical fracture of this curtain has revealed the pigment in section, providing the opportunity to sample for both minimum and maximum ages. ARD 14 was drilled from the middle of the curtain, and represents a maximum age for the pigment. It consists of a single sample. ARD 15 is carbonate formed on top of the pigment, and therefore represents a minimum age. It consists of two sub-samples, and based on a visual assessment of the formation they are expected to be approximately the same age as each other.

ARD 16 dates pigment applied to the edge of curtain 5 (Figs. S33, S34) and was sampled using both a hand-drill and scalpel. It consists of three sub-samples of carbonate overlying the pigment and therefore represents a minimum age. A lack of space made sampling difficult and the growth direction of the curtain was not clear, therefore this sequence may not be strictly in stratigraphic order.

3.3.2 Drapery between Panels III-C-2 and III-C-3, samples ARD 26 - 28

A layer of red pigment is visible in the section of broken drapery between Panel III-C-2 and III-C-3. Samples ARD 26 - 28 provide minimum and maximum ages for this pigment (Fig. S35), all of which were collected by drilling.

ARD 26 consists of two sub-samples taken from immediately overlying the pigment, and therefore provides a sequence of minimum ages. ARD 27 (a single sample) also provides a minimum age, but consists of carbonate from several layers above the pigment and so formed after ARD 26. ARD 28 (a single sample) was taken from ~2 mm beneath the pigment and therefore represents a maximum age for its application.

3.3.3 Red pigment line in cross section of a curtain Panel II-C-8, samples ARD 6 to 10

Red paint on this curtain was partly covered by later continued growth of the formation situated in Panel II-C-8. A breakage exposed the cross section and the red paint on the surface extends as a clearly visible red layer interstratified with the carbonate formation (Fig. S10 and S37) Fig. S36 shows the cross section of the curtain, exposed by the breakage, before sampling and Fig. S38 shows details and the positions of samples ARD 6 to 10. Samples ARD 6, 7 and 10 are drilled from the curtain underlying the red paint and yield maximum ages for the painting.

ARD 8 and 9 are drilled from the curtain formation above the paint and yield minimum ages for the painting.

Supplementary Text

1. U-series results

1.1 La Pasiega

A total of 21 carbonate crusts from La Pasiega C have been analysed so far. Fourteen results were previously published, nine in Pike et al (*17*) and five in Hoffmann et al. (*14*). For this study, we analysed another seven crusts. All analytical results are provided in Table S4.

The quality of the dated material from La Pasiega is generally very good. The carbonate crusts were pristine and visibly clean. There were no indications of alteration. For all samples presented here, no residuals were found after dissolution and chemical sample preparation and purification, and MC-ICPMS analyses were all successful. The U concentration of the samples presented in this study ranges between 0.1 and 1.8 µg/g. This range is a bit wider but similar to the previously reported range between 0.4 and 1.5 µg/g (*14*). The $^{234}U/^{238}U$ activity ratios are generally elevated, with values between 2.28 and 4.25, confirming the previously described elevated ratios for this cave.

For most samples the $^{232}Th/^{238}U$ activity ratio is below 0.01 and detrital contribution not significant. However, the sample PAS 34, most relevant for this study, has elevated $^{232}Th/^{238}U$ activity ratios. We were able to take three sequential samples (PAS 34 a, b, c). The dense and pristine carbonate had some dust on the surface and appeared greyish, but the surface cleaning revealed white carbonate. No indication of pigment was found on top of the carbonate. The surface was cleaned, three visibly clean sub-samples were taken, and pigment was then clearly revealed underlying the sampling spot.

There are slightly elevated levels of detrital ^{232}Th in samples a and b with $^{232}Th/^{238}U$ activity ratios of 0.05 ($^{230}Th/^{232}Th$ of 33 and 28, respectively). Sample PAS 34c has a significant degree of detrital contamination with $^{232}Th/^{238}U$ activity ratios of 0.28 ($^{230}Th/^{232}Th$ of 7.3). A bulk earth value of the upper crust ($^{238}U/^{232}Th_{act} = 0.8 \pm 0.4$) is used for detrital correction (see below). The dating results for the three sub samples are in strict stratigraphic order. The outermost sample PAS 34a returned an age of 51.6 ± 1.1 ka and the subsequent sample PAS 34b returned an age of 54.4 ± 1.4 ka. Uncorrected and corrected U-Th ages of the two samples PAS 34a and PAS 34b overlap within uncertainty. Even based on just these two results, obtained on samples with no significant detrital correction, the underlying art pre-dates arrival of modern humans in the Iberian Peninsula with a minimum age of 53 ka based on PAS 34b. Detrital correction for PAS 34c yields a corrected age of 79.7 ± 14.9 ka. This sample, which is closest to the pigment, has a high degree of detrital components and thus a significant

uncertainty for the corrected age. The minimum age for the painting based on PAS 34c is 64.8 ka. Uncorrected and corrected U-Th ages also overlap within uncertainty for PAS 34c, albeit the uncertainty of the corrected age is large due to propagated uncertainties of the detrital correction.

In most cases for samples from La Pasiega C a detrital correction is small and not significant. For all PAS samples we apply a detrital corection using the conventional bulk earth value, i.e. we assume a detrital $^{238}U/^{232}Th$ activity ratio (correction factor) of 0.8 with 50% uncertainty and a ^{238}U decay chain in the detrital component in secular equilibrium. This value is used because we do not have isochron-based initial $^{230}Th/^{232}Th$ activity ratios for carbonates in La Pasiega. Furthermore, there were no residuals left after sample digestion to assess a residual detritus-based correction factor.

For this study, the most relevant sample from La Pasiega is PAS 34. While PAS 34a and PAS 34b have relatively low detrital contamination, PAS 34c has a significant detrital component with ^{232}Th concentration of 153 ± 7 ng/g compared to ^{238}U concentration of 178 ± 8 ng/g and a $^{230}Th/^{232}Th$ activity ratio of 7.3 ± 0.1. Here, the correction is significant. This sub-sample can be used to constrain the maximum upper range of the detrital correction factor to 3.57 (the measured $^{238}U/^{232}Th$ activity ratio is 3.57). In case of this value, all U in the sample would be a result of detritus, a quite unrealistic scenario. Thus, the correction factor for La Pasiega samples has to be significantly smaller than 3.57 and we use the conventional bulk earth value of 0.8 ± 0.4.

To demonstrate that this correction factor is appropriate, we compare corrected results for PAS 34 using two different correction factors of 0.8 ± 0.4 and 2.0 ± 0.4. For PAS 34a this yields corrected ages of 51.6 ± 1.1 ka and 50.1 ± 1.1 ka, respectively. For PAS 34b this yields corrected ages of 54.4 ± 1.4 ka and 52.6 ± 1.5 ka. For PAS 34c we obtain corrected ages of 79.7 ± 14.9 ka and 69.9 ± 25.2 ka. The $^{234}U/^{238}U$ isotope ratio is also affected by detrital correction. The measured, uncorrected initial and corrected initial $^{234}U/^{238}U$ activity ratios are used to assess how realistic a correction factor higher than 0.8 would be. The values for all samples from Pasiega C are shown in Fig. S39. The measured $^{234}U/^{238}U$ for PAS 34 range between 3.467 and 3.8 (Fig. S40). Using a correction factor of 0.8, the corrected $^{234}U/^{238}U$ activity ratios for the three sub-samples of PAS 34 fall between 3.8 and 4.2, the resulting calculated initial $^{234}U/^{238}U$ activity ratios are between 4.26 and 4.9. For all other samples from La Pasiega C, where a detrital correction is not significant, the initial $^{234}U/^{238}U$ activity ratios, derived from the corrected $^{234}U/^{238}U$ activity ratios, range between 2.16 and 5.12, so the correction value of 0.8 yields initial $^{234}U/^{238}U$ activity ratios for PAS 34 within the range of all

results from this part of the cave. A higher correction factor, e.g. > 2 yields an initial $^{234}U/^{238}U$ activity ratio > 10 for PAS 34c, well outside any other value for the cave and unrealistic different to all other samples.

1.2 Maltravieso

Samples from Maltravieso can have significant levels of detrital contamination with $^{230}Th/^{232}Th$ activity ratios as low as ~5 (Table S4), meaning that in some cases the detrital correction is significant. No insoluble residues from the carbonate samples were present after dissolution, so it was not possible to characterise the composition of the detrital component through direct analyses of insoluble fractions. Instead, three sediment samples were collected from within the cave. These were analysed following the methodologies detailed above, with soluble and insoluble fractions processed separately. The mean measured $^{232}Th/^{238}U$ activity ratio, regarded as a good proxy for the detrital component of the carbonate samples, was then used for the detrital correction of samples from this cave: $^{238}U/^{232}Th = 3.3 \pm 0.2$ (errors are given as 2σ standard errors of the mean, n = 3). This value represents the combined, mass-balanced, soluble and insoluble fractions. Due to the dominance of the soluble fraction (>95 % total mass of each sample) this value would be the same if only the $^{238}U/^{232}Th$ activity ratios of the soluble fractions were used. Activity ratios for the $^{230}Th/^{238}U$ and $^{234}U/^{238}U$ are again assumed to be = 1.0.

To test the applicability of this correction, a section of a fractured stalagmitic column (MAL 24, Fig S41) was sampled from the Sala de las Pinturas. Six carbonate layers, representing a stratigraphic sequence through the stalagmite, were hand-drilled to produce powders for dating (MAL 24A–F). $^{230}Th/^{232}Th$ activity ratios ranged from 5 to 120 highlighting differing degrees of detrital contamination for different layers. When detrital corrections employ an assumed detrital activity ratio of $^{238}U/^{232}Th = 0.8 \pm 0.4$, typical of upper crustal silicates (*51*), sample MAL 24F (third from the core, $^{230}Th/^{232}Th$ activity ratio of 5.25) falls out of stratigraphic order. When detrital corrections employ the (sediment) measured detrital activity ratio of $^{238}U/^{232}Th = 3.3 \pm 0.2$, all samples fall in stratigraphic order within error (Fig. S41). This suggests that: 1) the assumed $^{238}U/^{232}Th$ activity ratio is not appropriate for detrital corrections on samples from this cave, and 2) the measured $^{238}U/^{232}Th$ activity ratio of the cave sediments is a better estimate of detrital values of the dating samples. All carbonate samples from Maltravieso are therefore corrected using the measured sediment detrital activity ratio of $^{238}U/^{232}Th = 3.3 \pm 0.2$. Note that this has the effect of making our corrected ages *younger* than if they were corrected using $^{238}U/^{232}Th = 0.8 \pm 0.4$.

The age of hand stencil GS3b has been constrained by dating five sample sequences: MAL 13, MAL 14, MAL 15, MAL 17 and MAL 19 (Table S4). MAL 13 consists of a pair of samples, with the inner most sample dating to 70.1 (+ 3.8 - 3.4) ka. This gives a minimum age of 66.7 ka for the stencil. The sample pair contains the surface cleaning sample in order to demonstrate that results are stratigraphically consistent. The remaining sample sequences are all stratigraphically consistent within error except for MAL 15A, however this case can be explained by the widening of the sampling area during collection of sub-samples B and C (Fig. S20) which would have incorporated increasing amounts of younger material from the outer layers of the cauliflower formation. The inner most sample of MAL 15, in total a sequence of six sub-samples, dates to 39.5 (+ 4.4 - 4.2) ka, giving a minimum age of 35.3 ka. MAL 14 is a set of three sub-samples, and provides a minimum age of 23.1 ka, whilst MAL 19, a set of two sequential sub-samples (once again including a surface cleaning sub-sample) provides a minimum age of 14.7 ka. MAL 17 is a sequence of four sub-samples, with the inner most sample dating to 63.6 (+ 9.6 - 8.4) ka. This gives a minimum age of 55.2 ka, and supports the Neanderthal attribution of hand stencil GS3b implied by the date by MAL 13.

The higher $^{238}U/^{232}Th$ activity ratio of 3.3 ± 0.2, derived from analysis of local sediment, is preferred for the detrital correction of samples from Maltravieso. Table S3 shows corrected ages for all samples from this cave for two scenarios of correction factors: i) the bulk earth value of the upper crust ($^{238}U/^{232}Th$ activity ratio = 0.8 ± 0.4) and ii) the mean value of the sediment analyses ($^{238}U/^{232}Th$ activity ratio of 3.3 ± 0.2). The data demonstrate that the choice of detrital value makes no difference to the stratigraphic consistency of any of the sample sets. It also does not affect any of our conclusions relating to Neanderthal authorship of the art even though using our preferred detrital correction ($^{238}U/^{232}Th$ activity ratio of 3.3 ± 0.2) yields younger corrected ages than if the bulk earth value is used.

1.3 Ardales

Samples from Ardales are characterised by minor levels of detrital contamination, as demonstrated by $^{230}Th/^{232}Th$ activity ratios >34 (Table S4). Following typical procedures, we therefore correct for detrital contamination using an assumed detrital activity ratio of $^{238}U/^{232}Th = 0.8 \pm 0.4$, typical of upper crustal silicates (*51*), and $^{230}Th/^{238}U$ and $^{234}U/^{238}U = 1.0$ (i.e. ^{230}Th, ^{234}U and ^{238}U isotopes are in secular activity equilibrium). However, the correction is minor and, except for ARD 06, all corrected and uncorrected ages overlap within their analytical uncertainties.

II-A-3 consists of a series of red painted curtain formations which have formed radiating from a large stalagmitic boss. The pigment is about 40 to 140 cm above the present day ground

surface. The boss is free standing and not connected to the cave wall and so isolated from possible sources of natural red oxide seeps. No red clays or minerals that could have been 'accidently' transferred to the drapery are visible on the present surface, nor were they present in layers excavated down to and including the Mousterian in the archaeological trenches a few meters away (Fig. S9).

These curtains have fractured at some point during antiquity revealing pigment in section, giving the opportunity to sample carbonate that provides both minimum and maximum dates for art. ARD 16 dates carbonate overlying pigment on curtain 5. Three sub-samples are stratigraphically consistent and provide a minimum age of 45.9 ka, indicating Neanderthal authorship. ARD 14 dates carbonate underlying pigment on curtain 6. A single date of 47.6 (+ 1.1 - 1.0) ka provides a maximum age for the art of 48.7 ka. ARD 15 dates carbonate that overlies this pigment. A pair of samples, stratigraphically consistent within error, provides a minimum age of 45.3 ka. The art on curtain 6 can therefore be constrained to between 48.7 and 45.3 ka, again predating the arrival of modern humans to Iberia. ARD 12 and ARD 13 both date carbonate overlying pigment on curtain 8. ARD 12 consists of a sequence of four sub-samples, however the outer sub-sample (46.4 ± 0.6 ka) is not stratigraphically consistent with the inner three, which range from 42.6 ± 0.6 ka to 43.8 (+ 1.9 - 1.8) ka. It was noted during sampling that sub-samples were not being taken in a strictly stratigraphic manner and the outer sample was removed from a much larger area (Fig. S26), so it is likely that these factors are behind the stratigraphic inconsistency outlined above. Bearing this in mind, and considering the outer sub-sample also overlies the pigment, it is this outer sample that actually gives the best approximation to the age of the art. As a result, a minimum age of 45.8 ka can be proposed. A further pair of sub-samples, ARD 13, provides a further minimum age for this pigment. The outer sample, 47.1 ± 0.6 ka, is broadly consistent with the dates from ARD 12. However, the inner sample indicates much older antiquity: 68.1 (+ 3.0 - 2.6) ka. Pigment on curtain 8 is therefore older than 65.5 ka. Two phases of art can be identified on this formation: one between 48.7 and 45.3 ka, as evidenced from the dating of curtain 6, and one prior to 65.5 ka as evidenced from the dating of curtain 8 (Fig. S42). Both predate the arrival of modern humans.

A layer of red pigment is visible in the section of broken drapery between III-C-2 and III-C-3. ARD 28 dates carbonate underlying this pigment and therefore provides a maximum age for the art: 42.5 (+ 3.1 - 3.0) ka. ARD 26 and ARD 27 date carbonate overlying the pigment and therefore provide minimum ages for the art. ARD 27 is located furthest from the pigment, consists of a single sample, and dates to 37.3 ± 1.3 ka. ARD 26 is located nearer to the pigment and consists of two sub-samples. These are stratigraphically consistent with each other and with

ARD 27 and ARD 28, with the inner of the two sub-samples dating to 40.4 ± 1.3 ka. The pigment on this formation can therefore be constrained to between 45.5 and 38.6 ka. This overlaps with the dating range of curtain 6 from II-A-3, so it is possible that both were applied at the same time (45.3 to 45.5 ka).

Red paint can be seen on a curtain in Panel II-C-8, which continues as a red layer interstratified between carbonate layers of the curtain, visible due to breakage. Samples were obtained from both overlying and underlying carbonate layers and constrain minimum and maximum age of the painting. The youngest sample of underlying carbonate yields a maximum age of 63.7 ka (ARD 06) and both samples taken from the overlying carbonate layer yield an identical minimum age of 32.1 ka (ARD 08 and ARD 09).

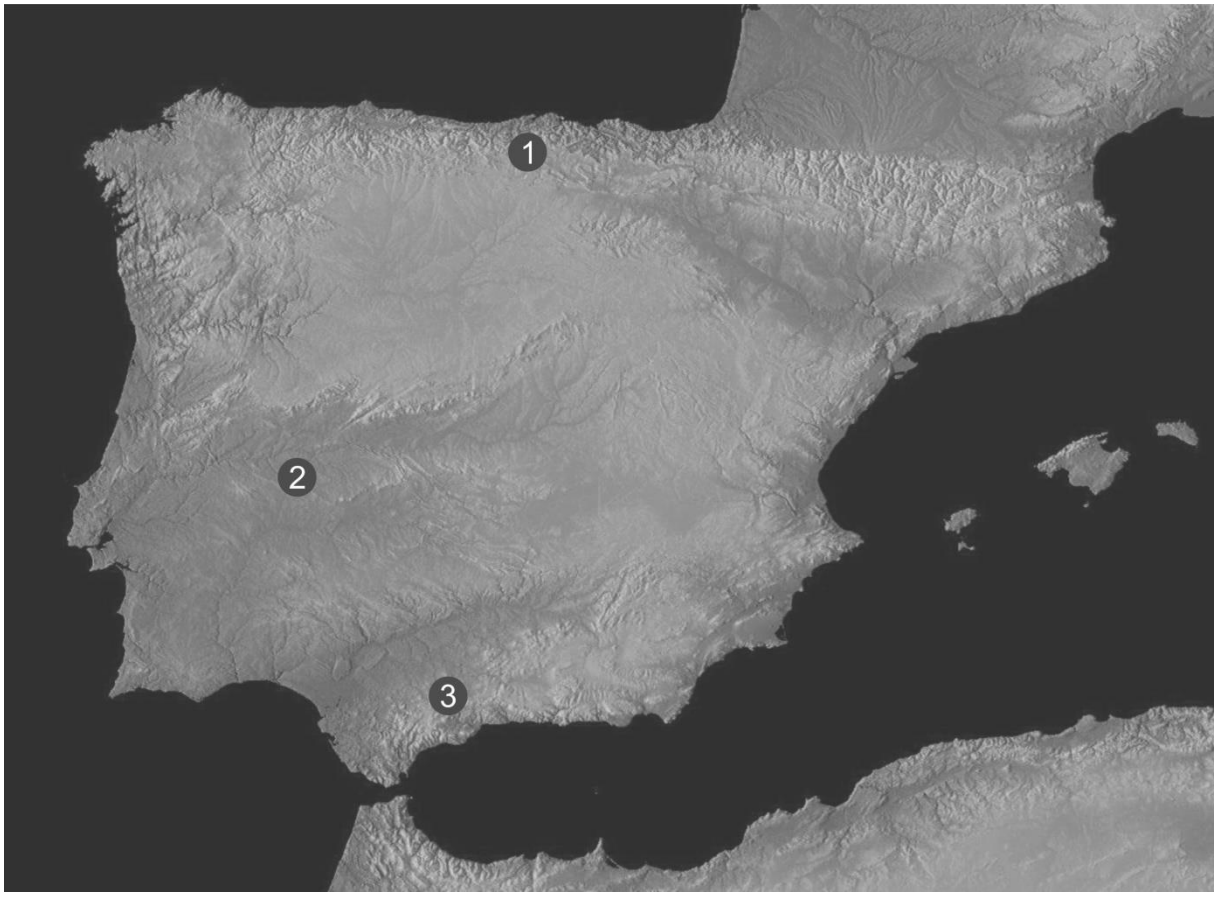

Fig. S1.

Map of the Iberian Peninsula. The dots indicate the locations of the three cave sites (1: La Pasiega, 2: Maltravieso, 3: Ardales).

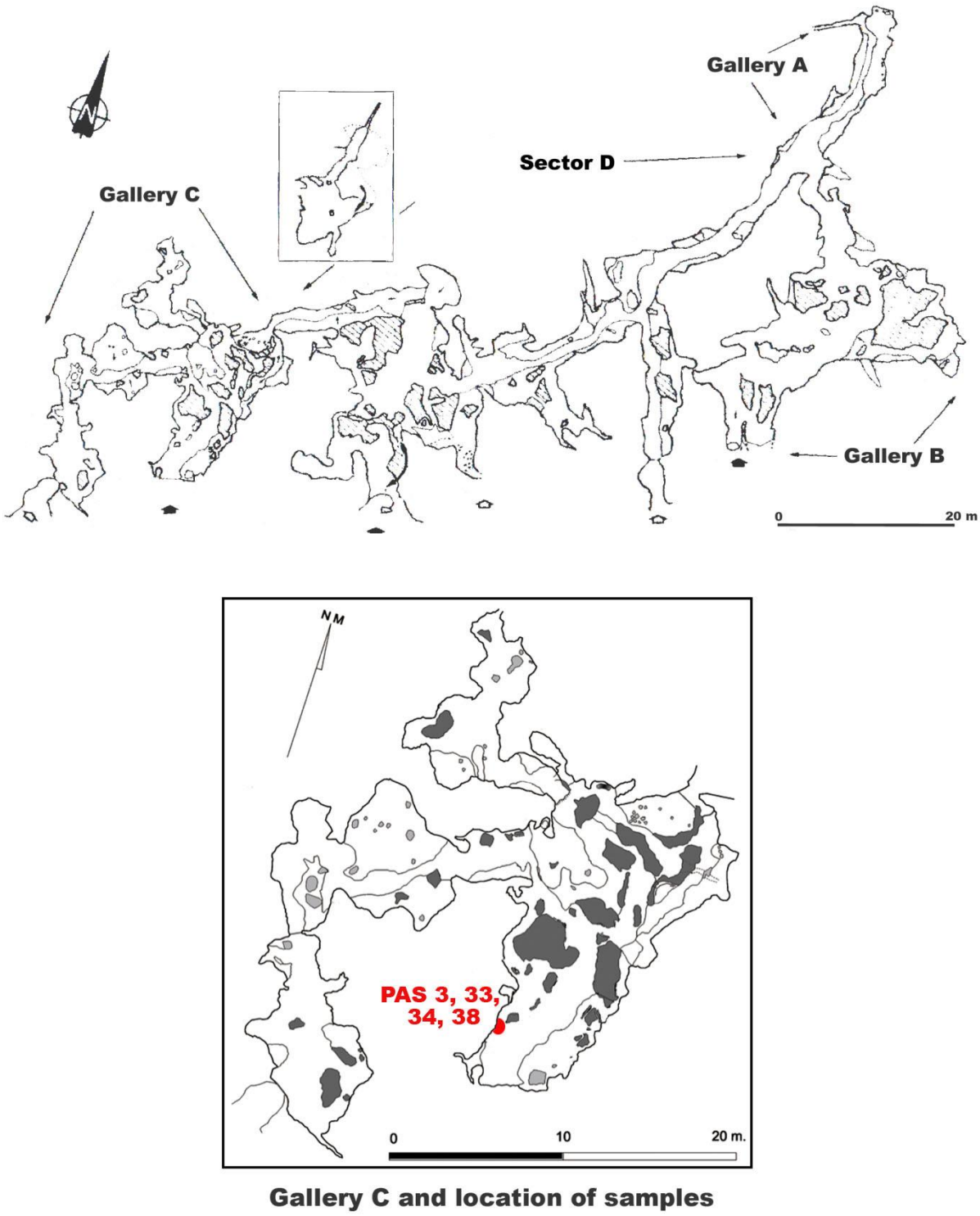

Fig. S2.

Top: Map of La Pasiega, indicating Galleries A, B and C. Bottom: Map of La Pasiega C, indicating the position of Panel 78, where samples PAS 3, 33, 34 and 38 were taken.

Fig S3.

Panel 78, La Pasiega C.

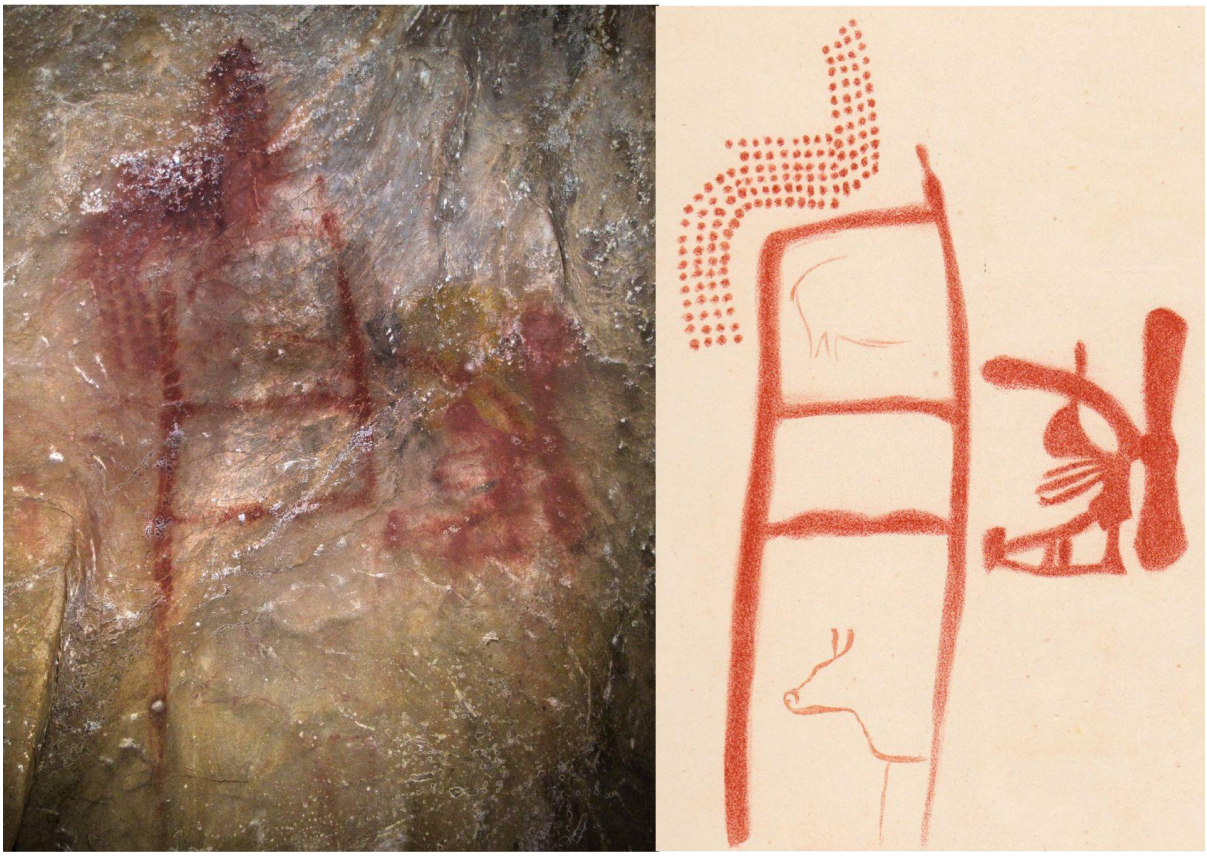

Fig. S4.

La Pasiega C, rectangular, scalariform motif with incomplete zoomorphs and red dots on Panel 78. Left: photo of the motif. Right: drawing by Breuil (taken from *(21)*).

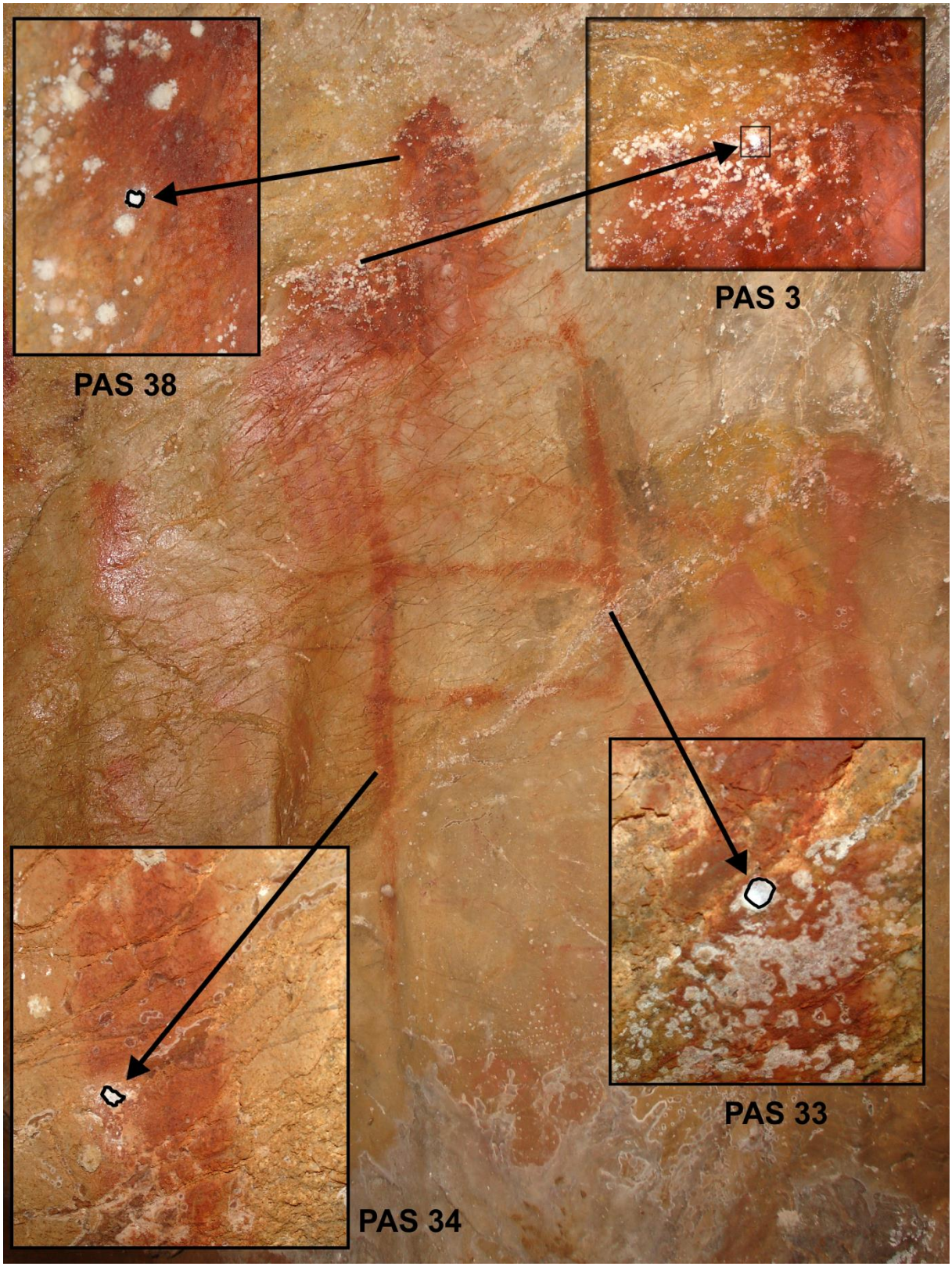

Fig. S5.

Detail of Panel 78, La Pasiega C (see also Fig. S3 and S4) indicating the positions of samples PAS 3, 33, 34 and 38 (see details for PAS 34 in (3.1.1)).

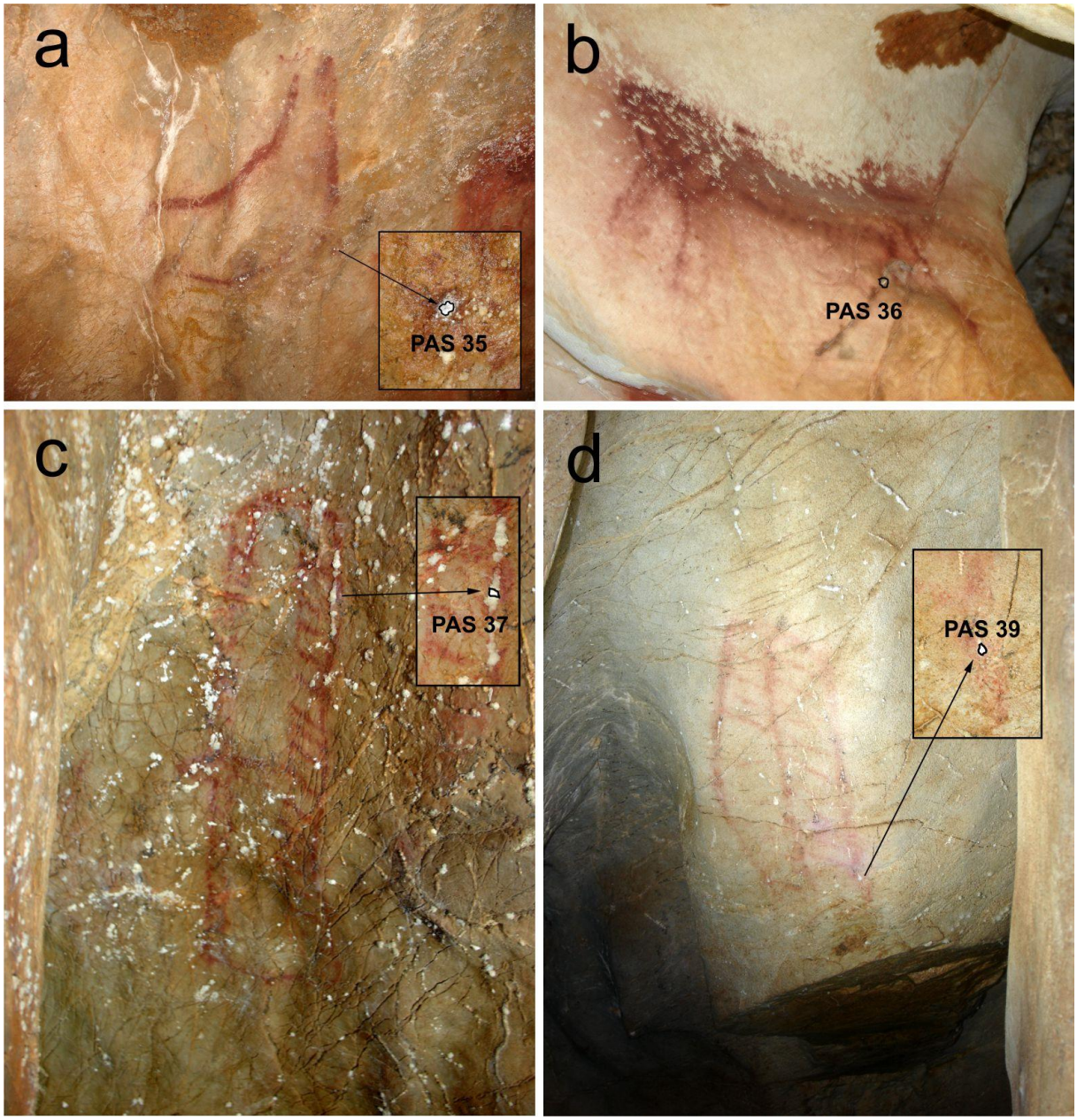

Fig. S6.

(a) incomplete red deer located in Panel 78. (b) carbonate-covered red zoomorph, classified as a hind by Breuil et al. *(21)* (Panel 82). (c) red tectiform (Panel 76). (d) red tectiform (Panel 72). Positions of samples PAS 35, 36, 38 and 39 are indicated.

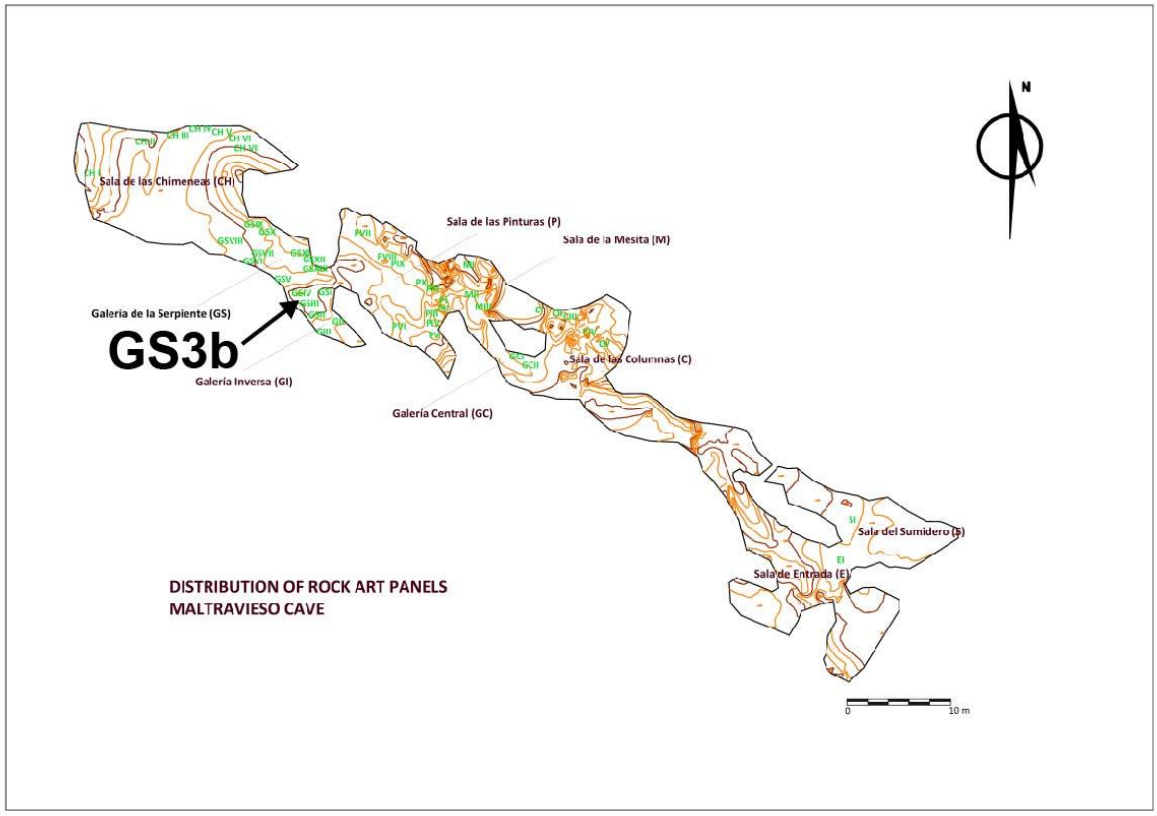

Fig. S7.

Map of Maltravieso cave. In green are the painted panels. Hand stencil GS3b is located in the Galería de la Serpiente.

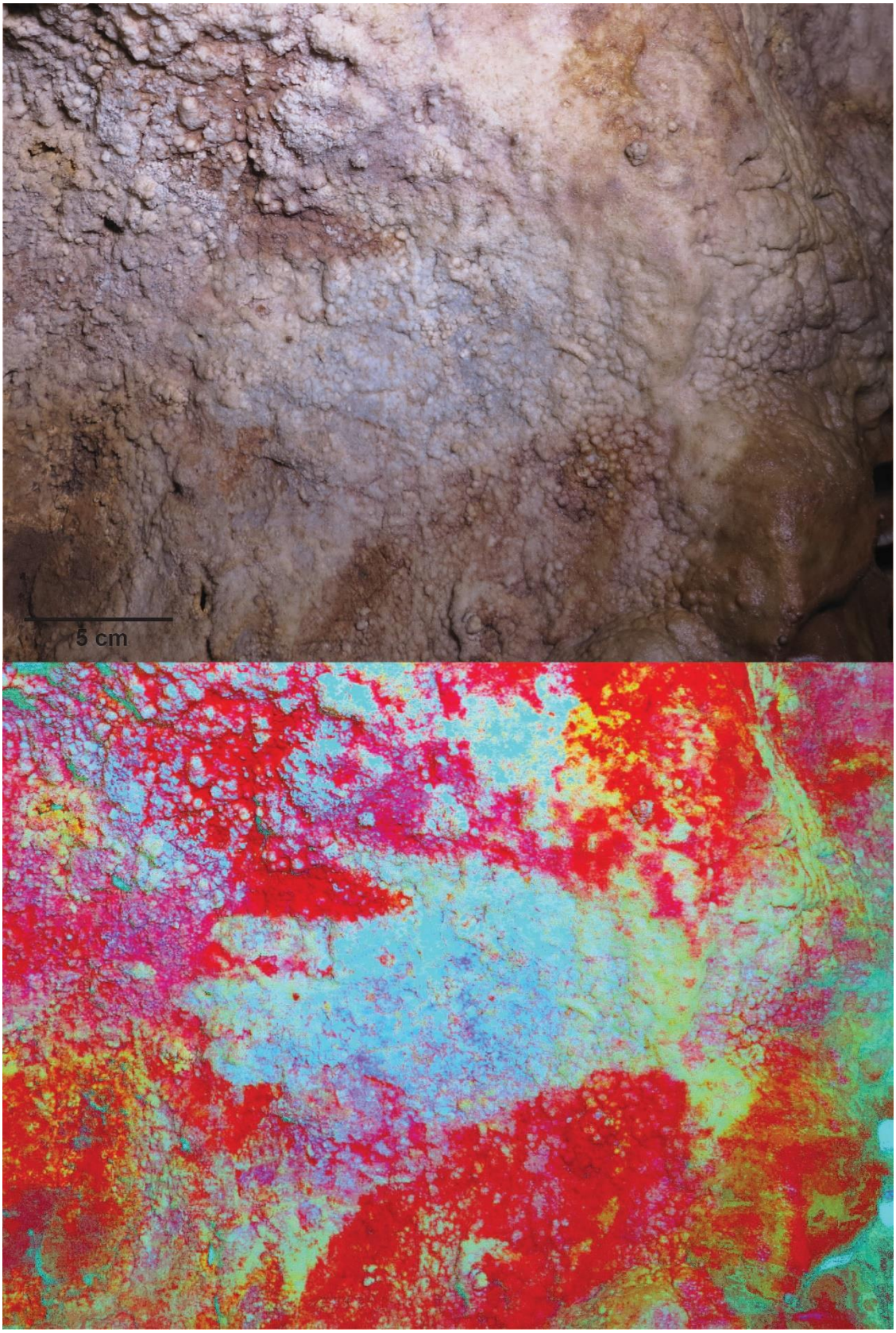

Fig. S8.

Hand stencil GS3b, Maltravieso cave, prior to sampling. The upper picture shows the original photo, the lower is the same picture after application of DStretch *(25)* (Correlation LRE 15%, auto contrast).

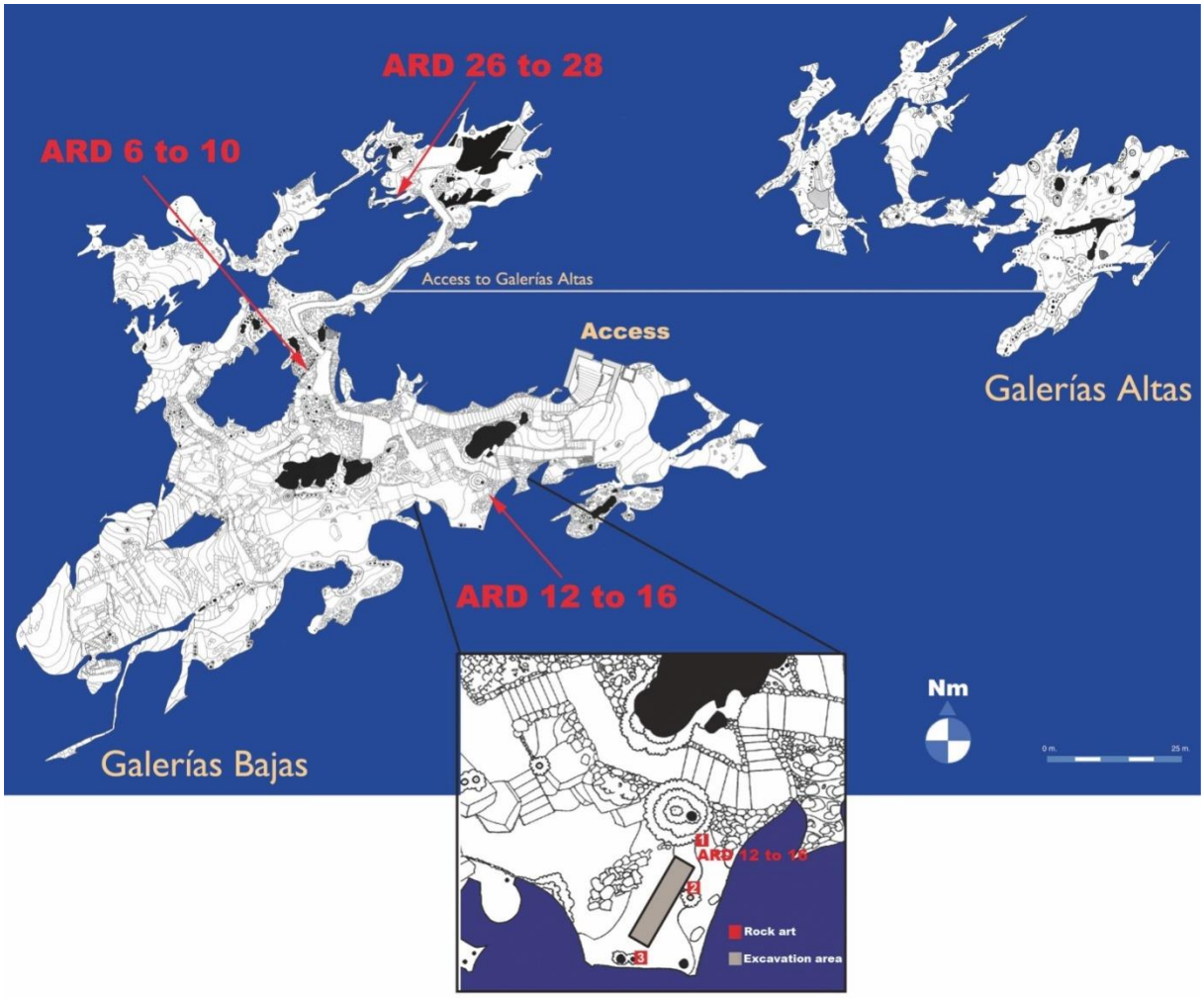

Fig. S9.

Map of Ardales cave. Positions are indicated of samples ARD 6 to 10 (Panel II-C-8); ARD 12 to 16 (Panel II-A-3) and ARD 26 to 28 (Panel III-C-2).

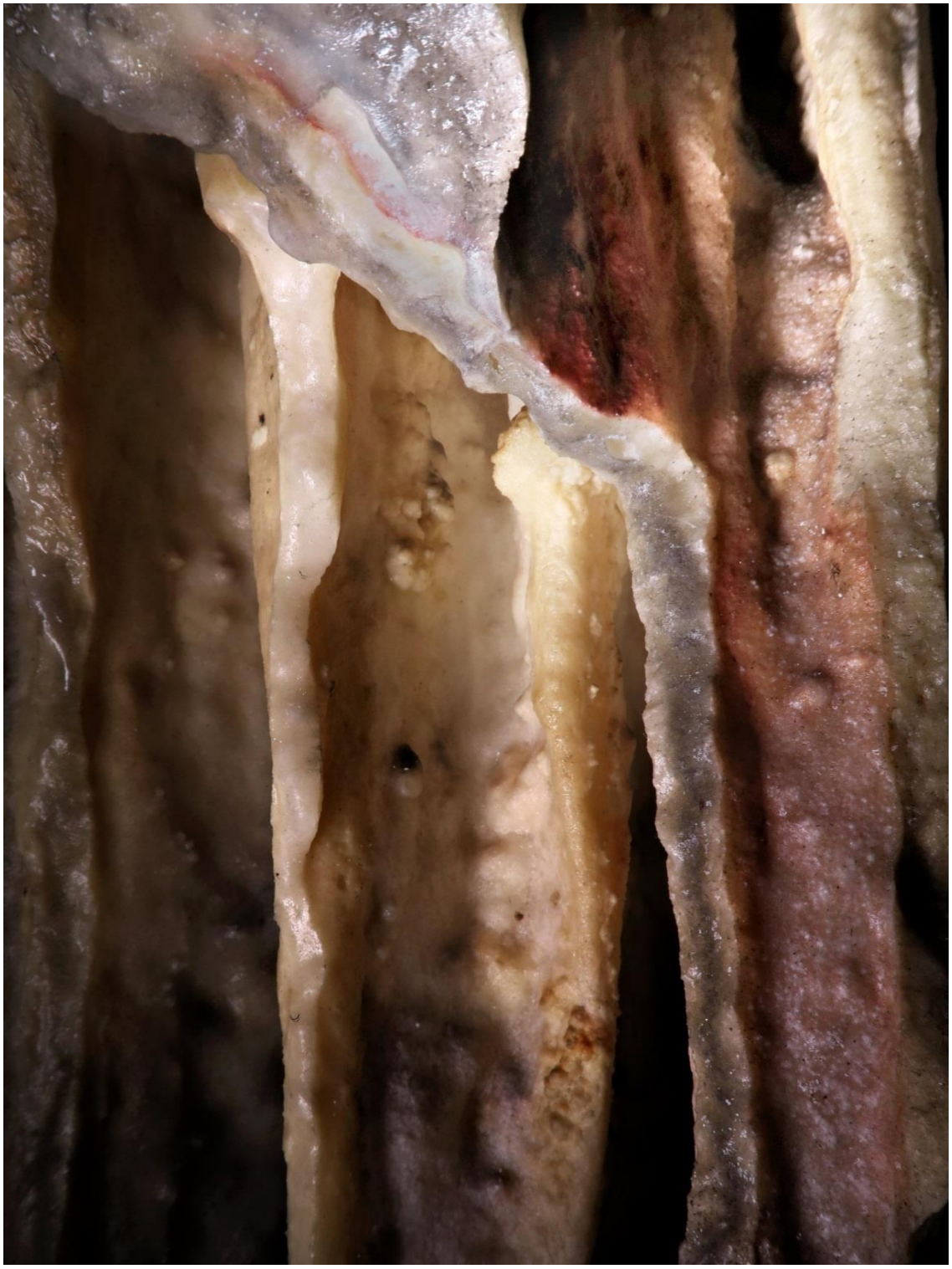

Fig. S10.

Broken section of a curtain formation, Panel II-C-8, Ardales. Red paint can be seen on top of the current surface to the right and above the break. In the top left area of the formation, the old surface, denoted by the red line of pigment visible in cross-section, was subsequently covered by continued speleothem growth (see details for ARD 6 - 10 in (3.3.3)). Overgrowth of painted surfaces, when revealed by such breakages, gives the opportunity to obtain maximum and minimum ages for the painting.

Fig. S11.

Curtain formation, Panel II-A-3, Ardales. Red paint can be seen on the curtain in the middle (see details for ARD 14 and 15 in (3.3.1)) and to the left.

Fig. S12.

Detail of a curtain formation, Panel II-A-3, Ardales. Note the red-painted old surface, incompletely covered by the subsequent accumulation of new carbonate layers (see details for ARD 16 in section 3.3.1).

Fig. S13.

Curtain formation, Panel II-A-3, Ardales. Red paint can be seen on the curtains in the middle and on the right (see details for ARD 12 and 13 (3.3.1)).

Fig. S14.

Broken curtain formation close to Panel III-C-2, Ardales. Red paint applied on a surface now completely covered by subsequent speleothem growth can be seen in cross-section as a thin red line (see details for ARD 26, 27 and 28 in (3.3.2)).

Fig. S15.

Sampling details for PAS 34. (a) Scalariform motif; the black rectangle denotes the area enlarged in (b). (b) The scalpel points onto the carbonate crust before sampling. (c) The carbonate crust after the surface was scraped for initial cleaning. (d) The carbonate crust after sampling, red pigment is visible in the centre, clearly underlying the remaining carbonate.

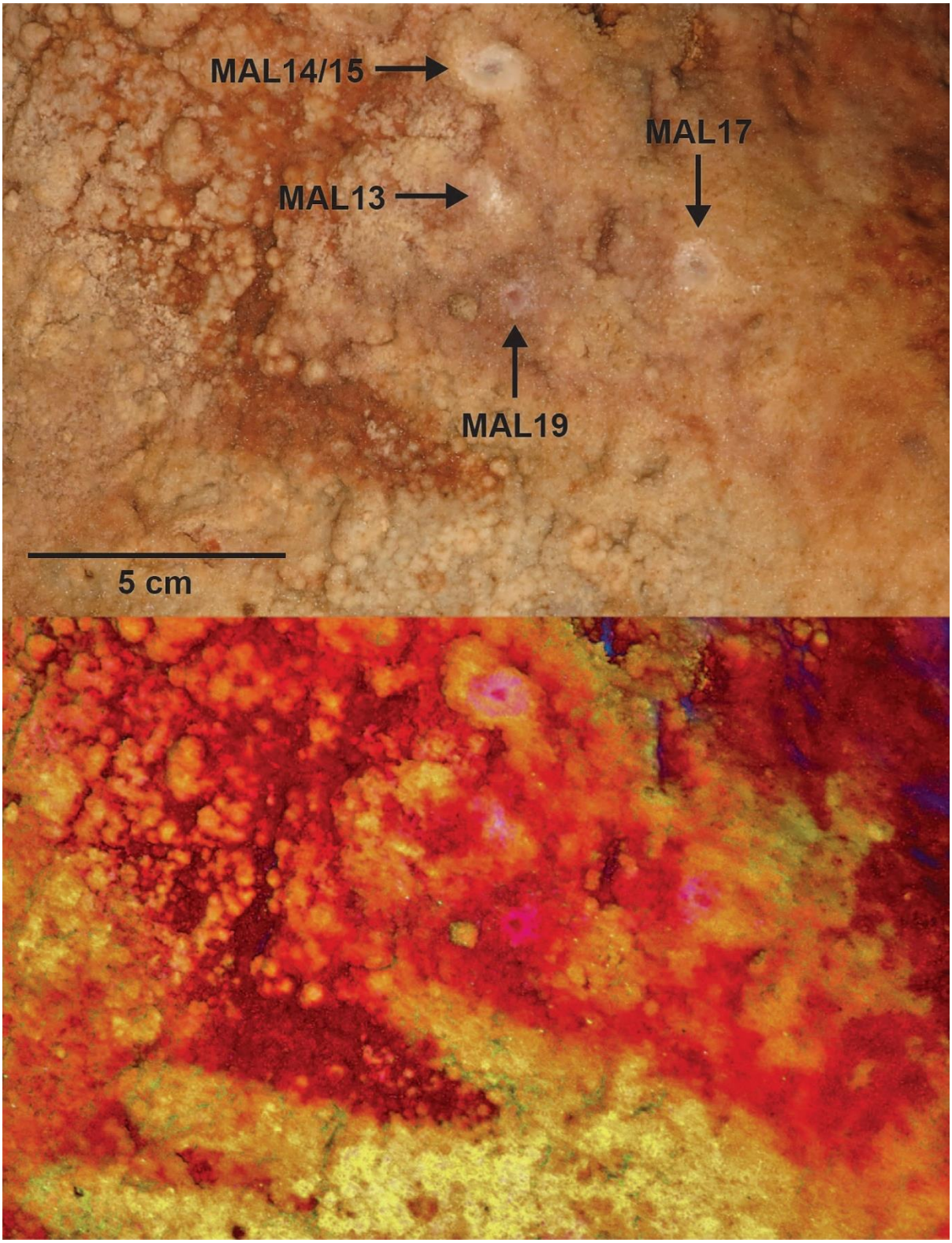

Fig. S16.

Sampling of hand stencil GS3b, Maltravieso. The upper picture shows the original photo with labelled sample locations, the lower is the same picture after application of DStretch (Correlation CRGB 15 %, auto contrast). Pigment is clearly visible in the valleys and cracks between carbonate growths.

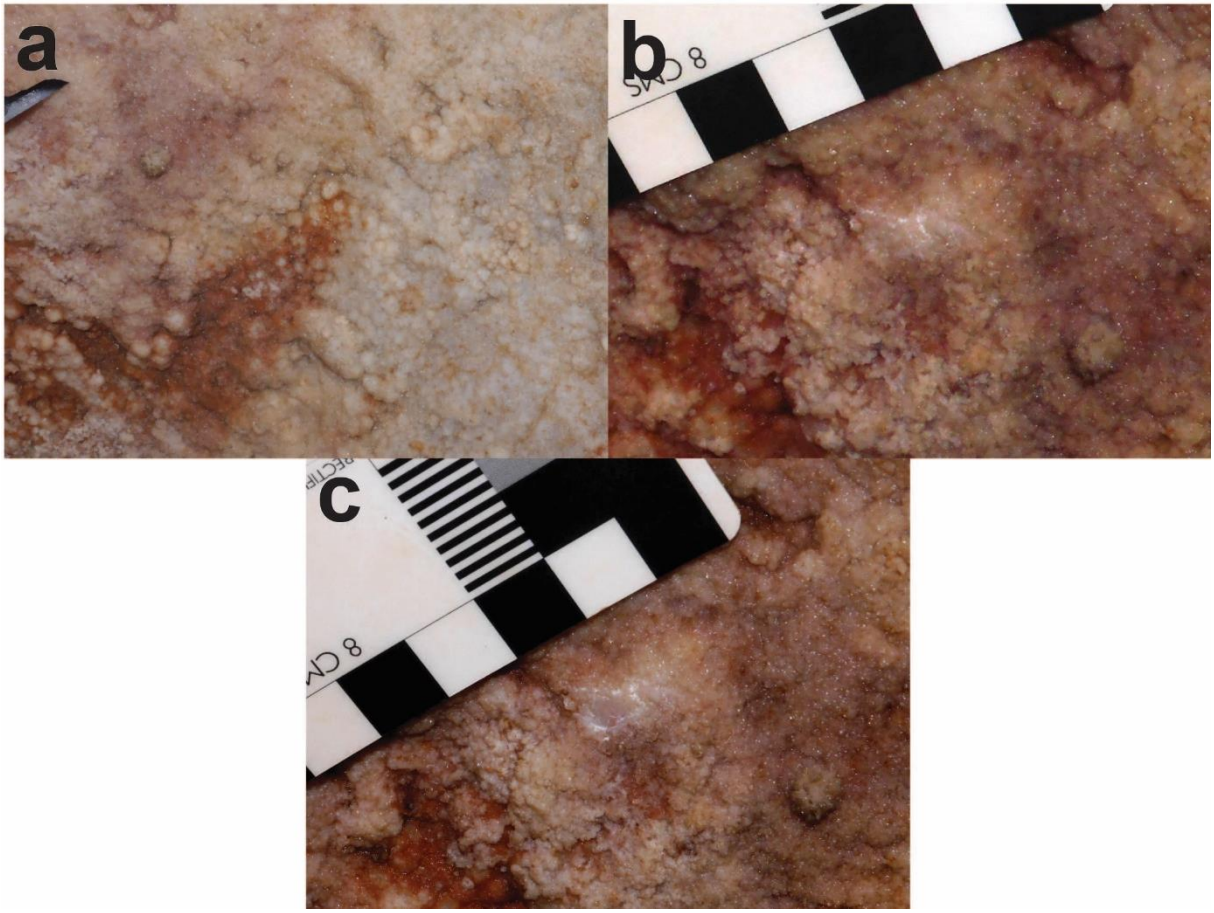

Fig. S17.

Details of sampling for MAL 13: (a) prior to sampling, (b) after surface cleaning, (c) after collection of MAL 13A.

Fig. S18.

Detail of MAL 13 after sampling. Pigment has become apparent in the bottom left of the sampling area.

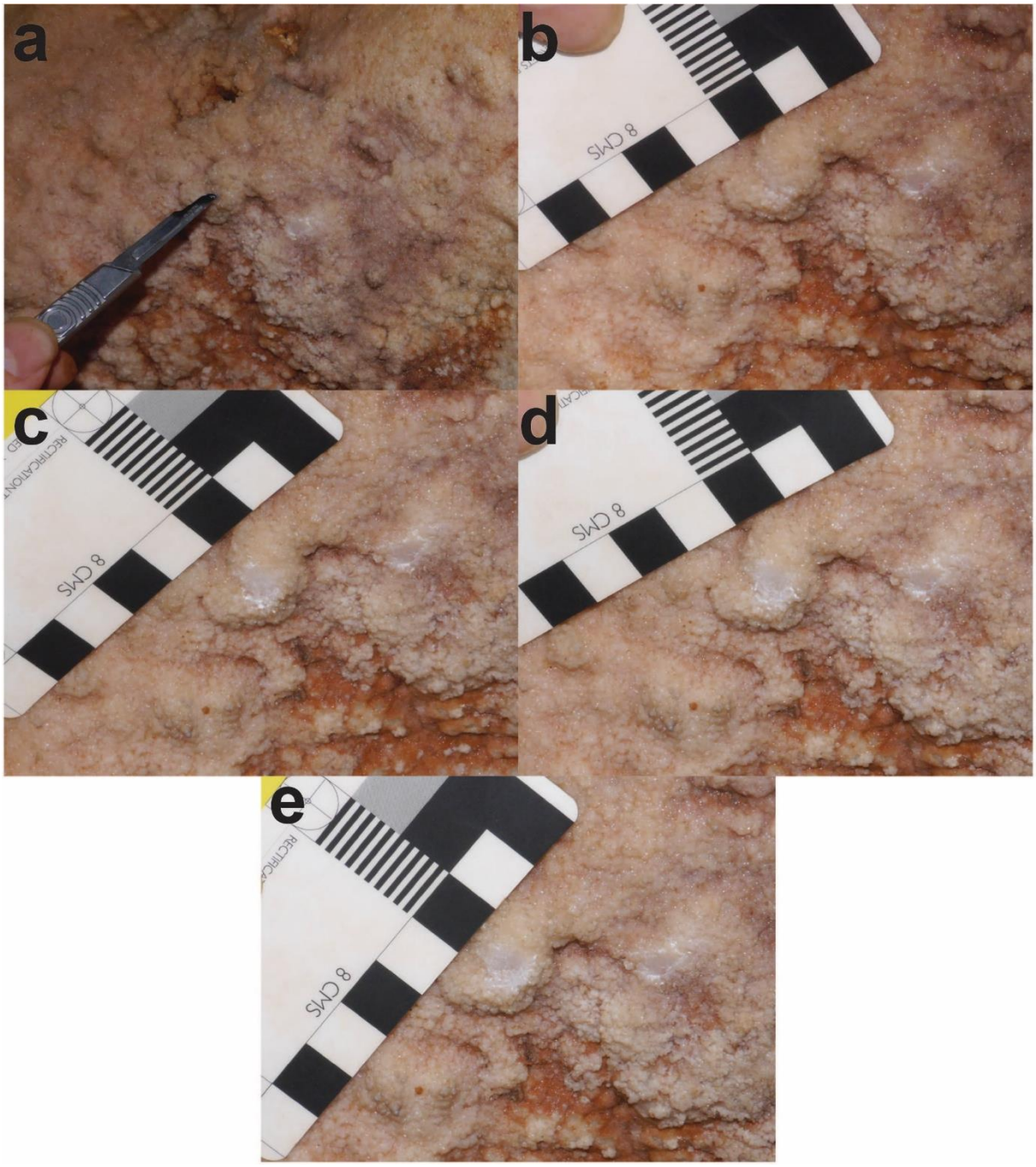

Fig. S19.

Details of sampling for MAL 14: (a) prior to sampling, (b) after clean, (c – e) after each sub-sample taken.

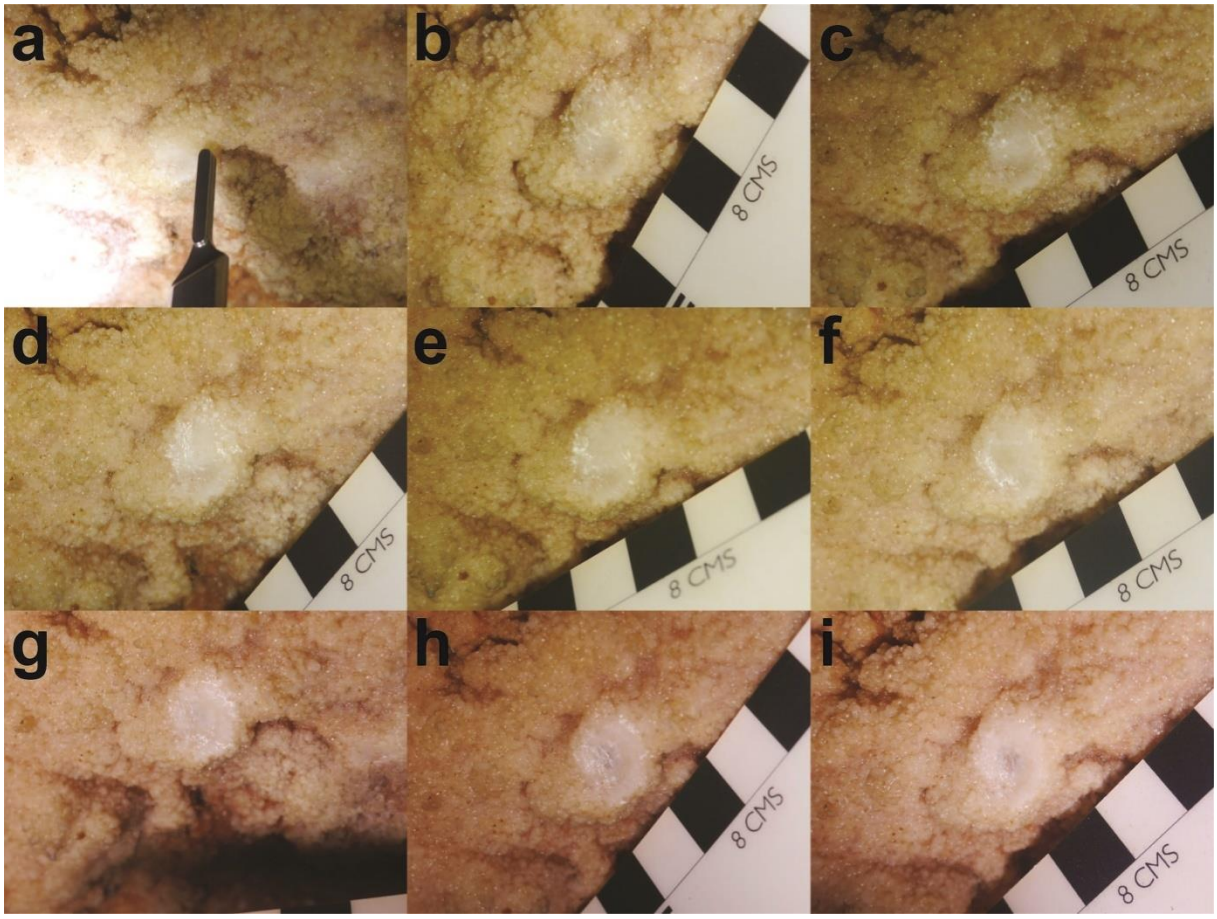

Fig. S20.

Details of sampling for MAL 15: (a) prior to sampling, (b) after clean, (c – h) after each sub-sample taken, (i) after final clean to confirm presence of underlying pigment. Note that the enlargement of the sample area during collection of sub-samples MAL 15B and MAL 15C (images d and e) explains the slight age inversion in this sequence.

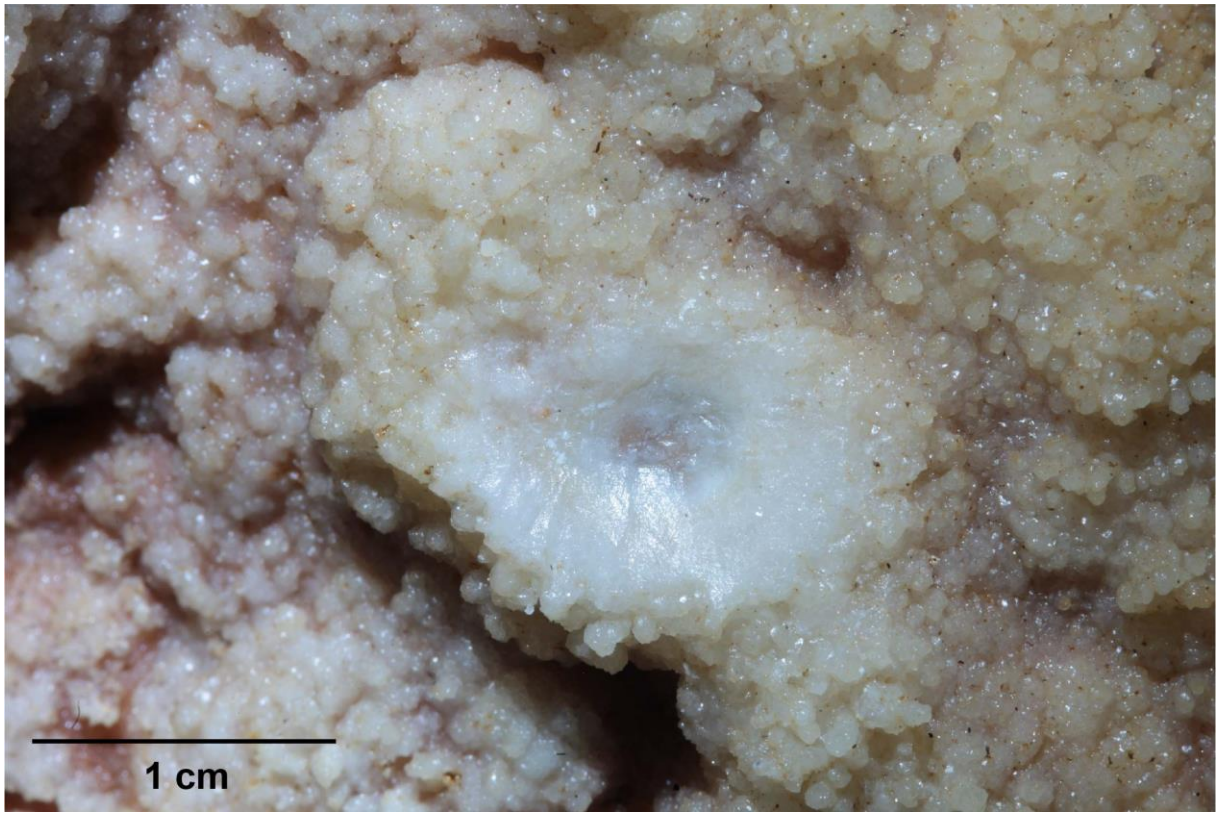

Fig. S21.

Detail of MAL 14 and MAL 15 after sampling. Pigment is showing through the layers of carbonate in the centre of the sampling area.

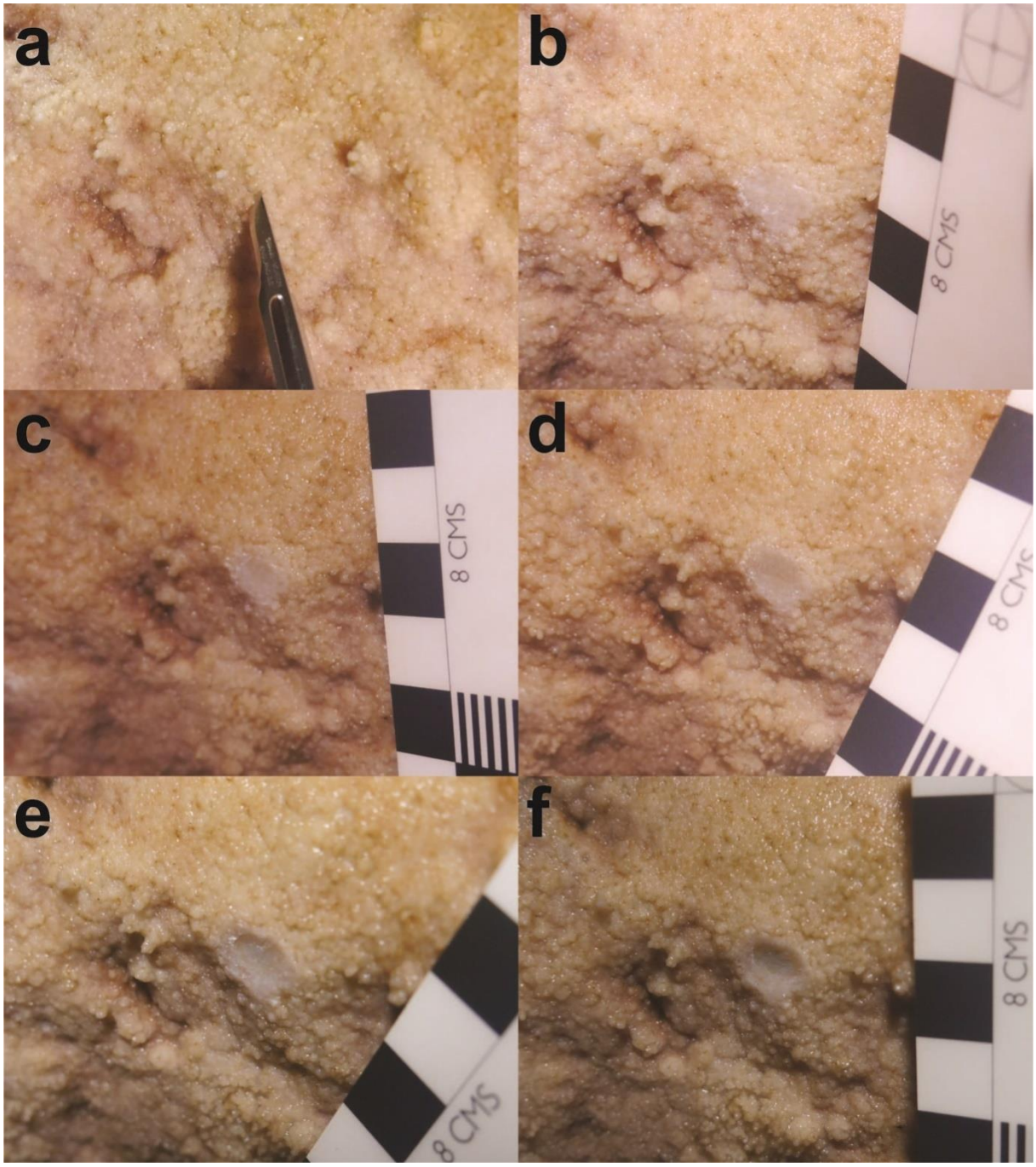

Fig. S22.

Details of sampling for MAL 17: (a) prior to sampling, (b) after cleaning, (c – f) after each sub-sample taken.

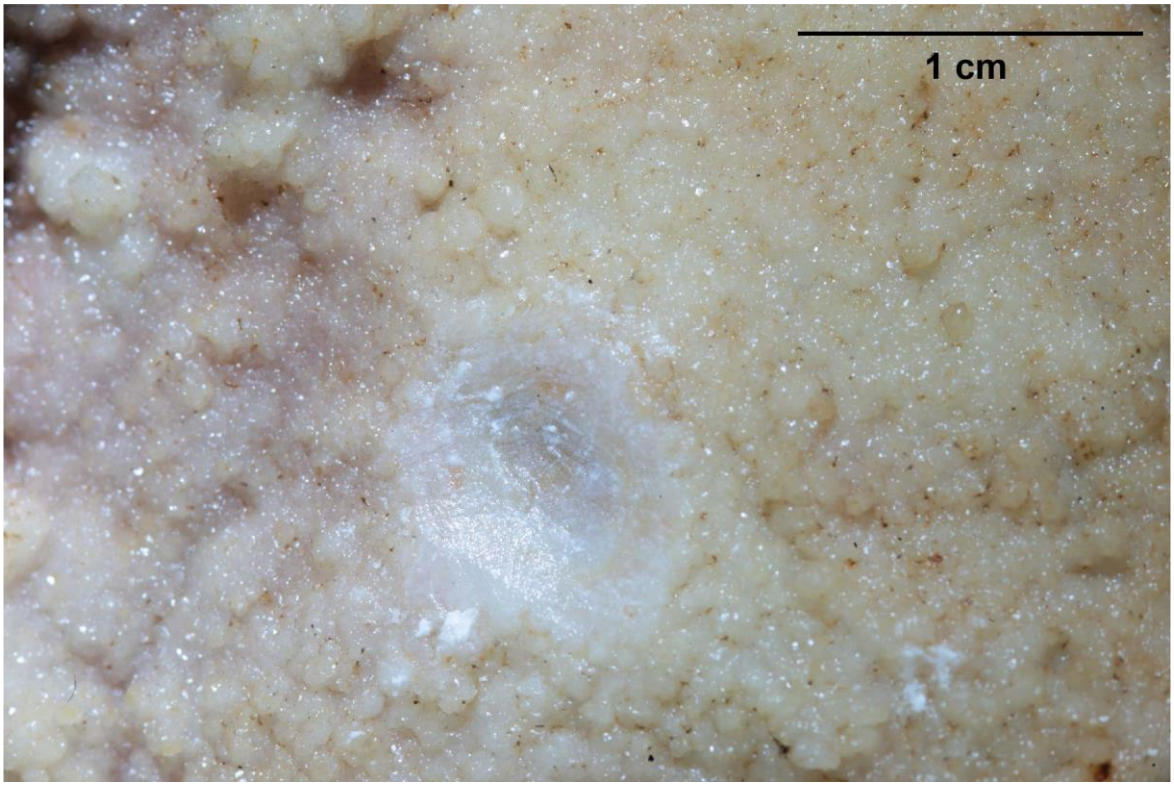

Fig. S23.

Detail of MAL 17 after sampling with pigment apparent below the carbonate in the centre of the sampling area.

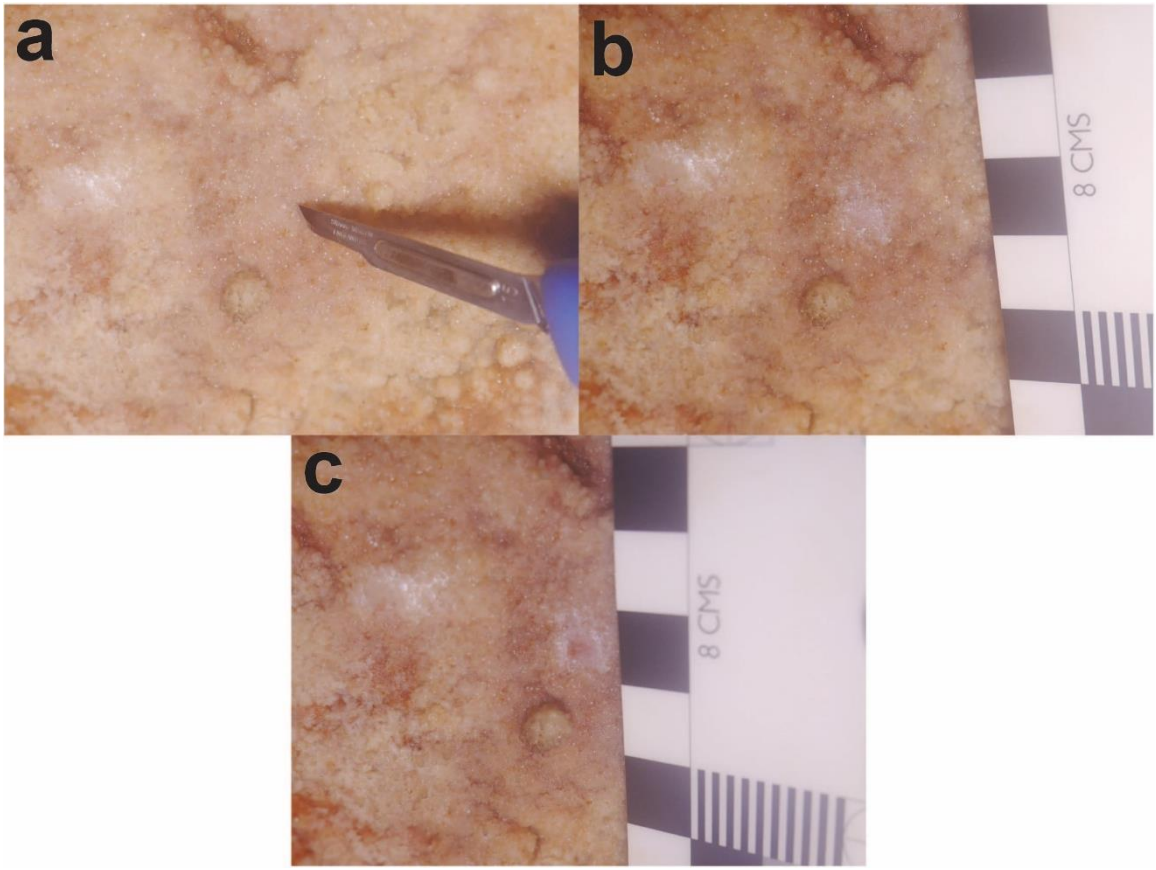

Fig. S24.

Details of sampling for MAL 19: (a) prior to sampling, (b) after cleaning, (c) after collection of MAL 19A.

Fig. S25.

Detail of MAL 19 after sampling. Sampling stopped when pigment became apparent below the lowest layers of carbonate.

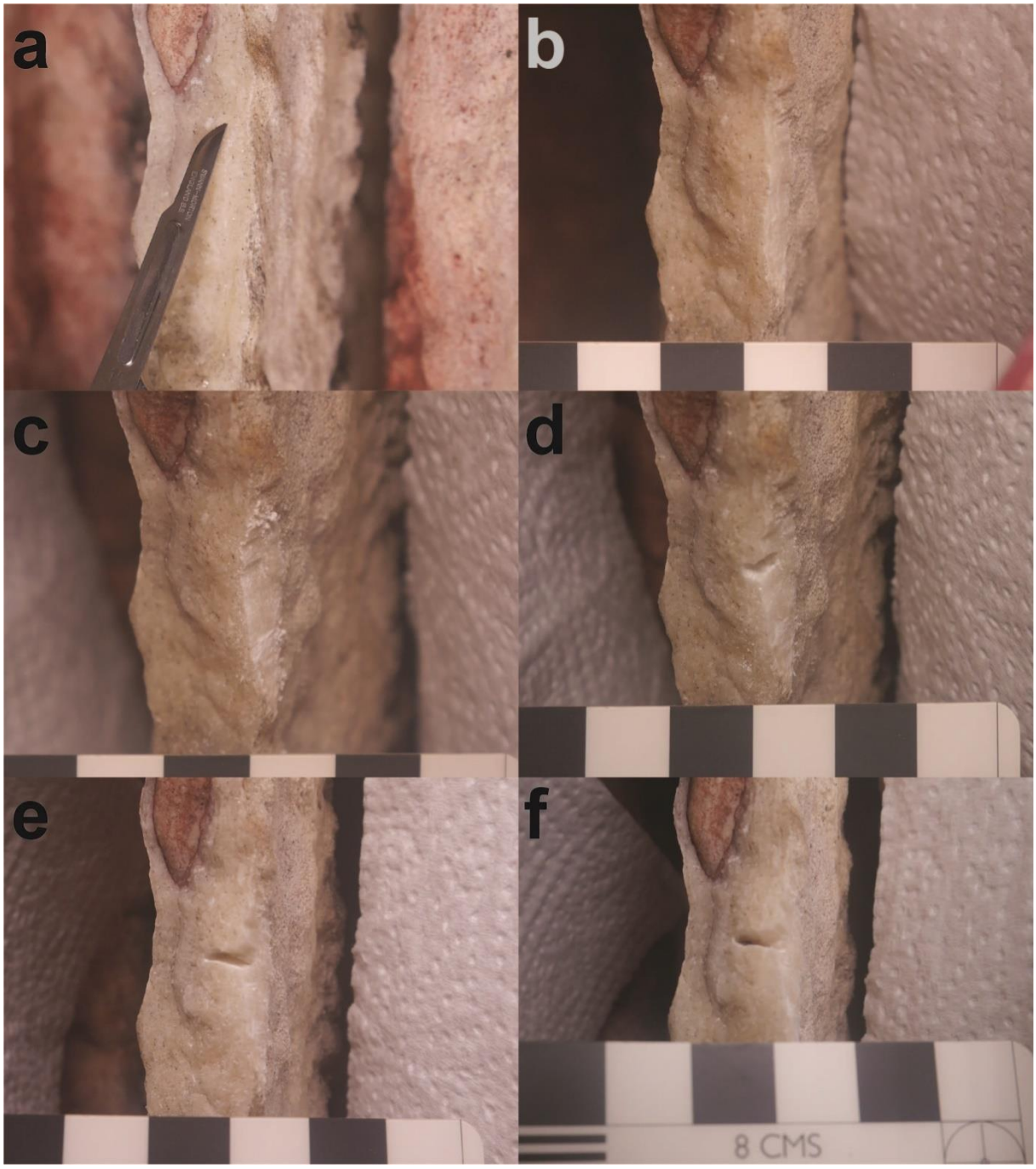

Fig. S26.

Details of sampling for ARD 12: (a) prior to sampling, (b) after cleaning, (c – f) after each sub-sample taken.

Fig. S27.

Detail of ARD 12 after sampling. Pigment is clearly visible towards the base of the sample area.

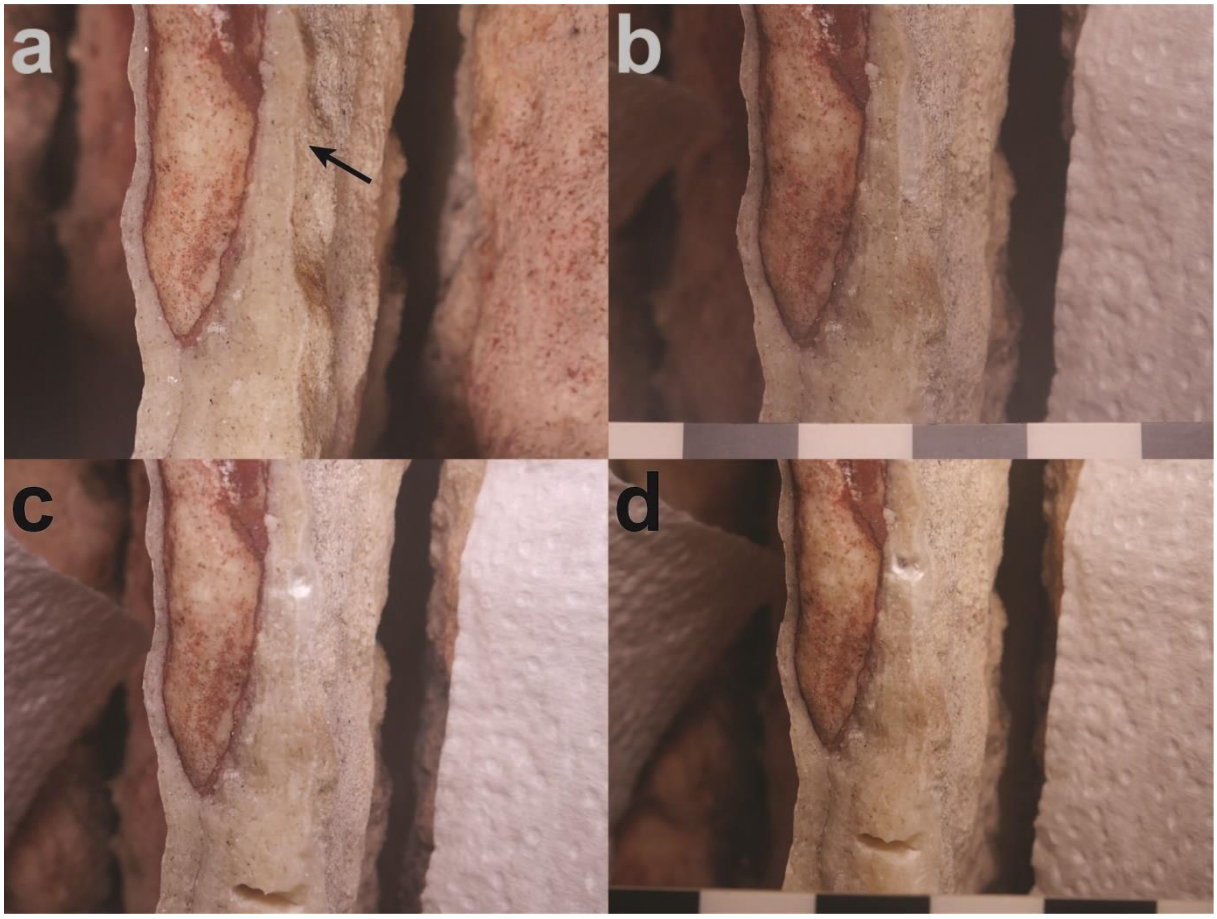

Fig. S28.

Details of sampling for ARD 13: (a) prior to sampling, (b) after clean, (c – d) after each sub-sample taken.

Fig. S29.

Detail of ARD 13 after sampling. Pigment is clearly visible towards the base of the sample area.

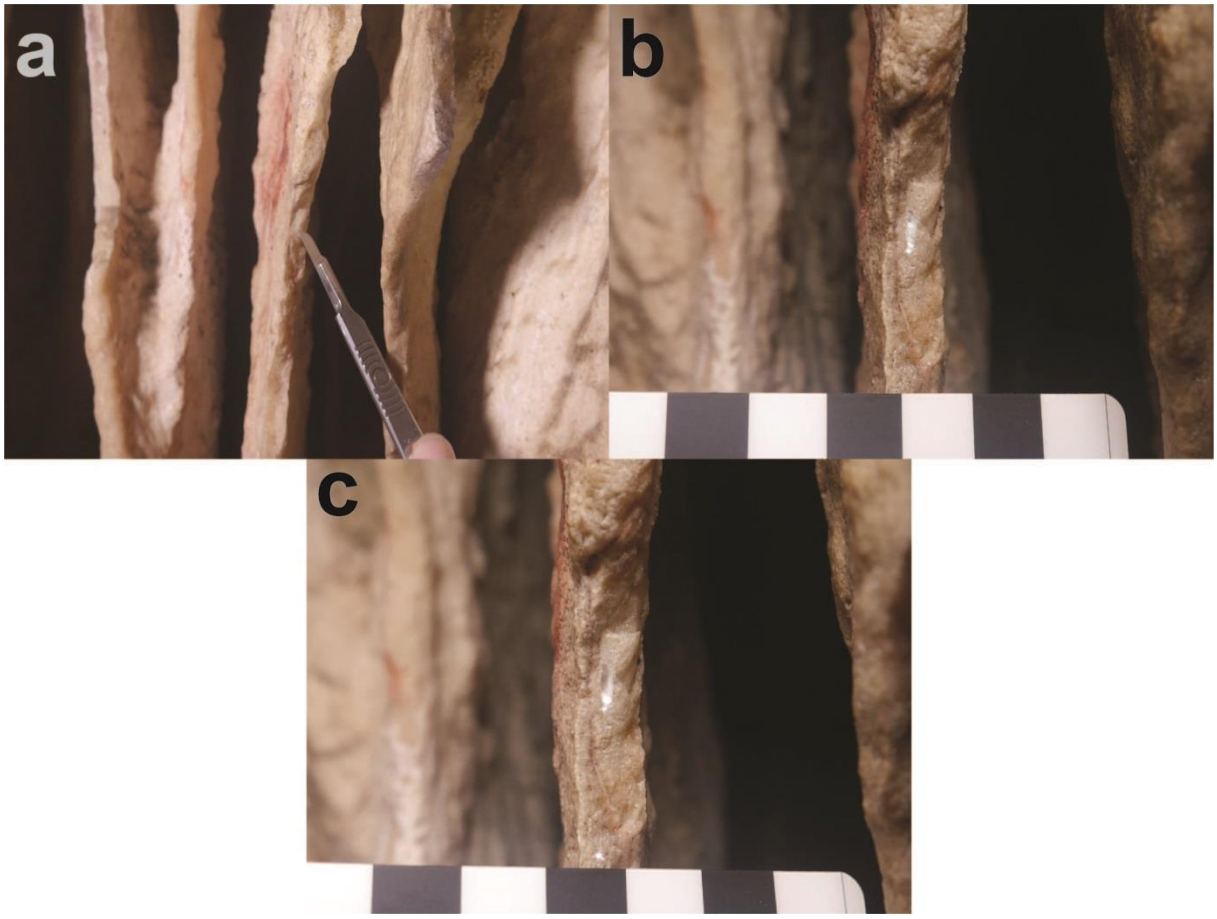

Fig. S30.

Details of sampling for ARD 14: (a) prior to sampling, (b) after cleaning, (c) after collecting sample ARD 14A.

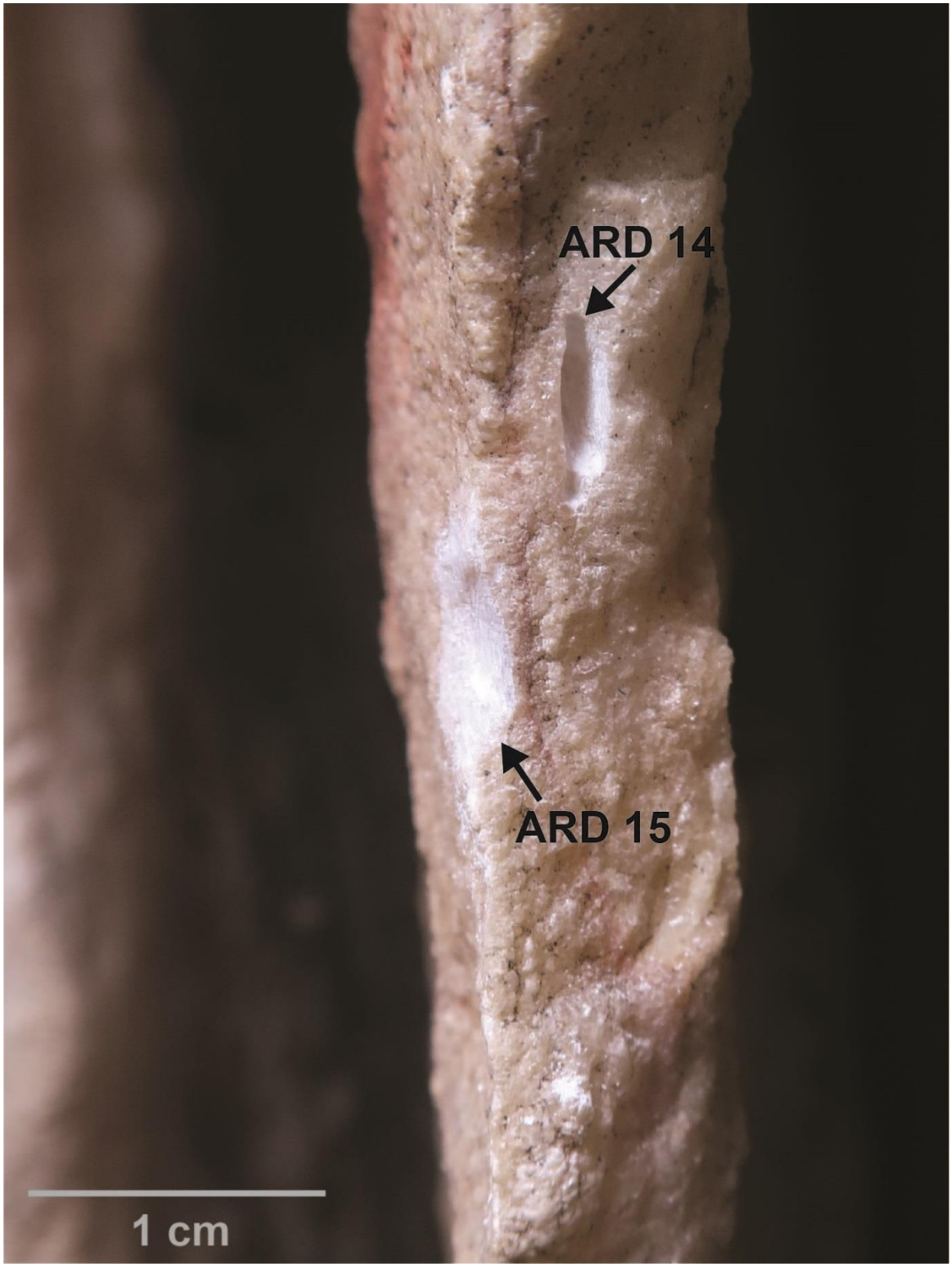

Fig. S31.

Details of ARD 14 and ARD 15 after sampling. The painted surface is seen as a line of pigment to the left of ARD 14 and to the right of ARD 15.

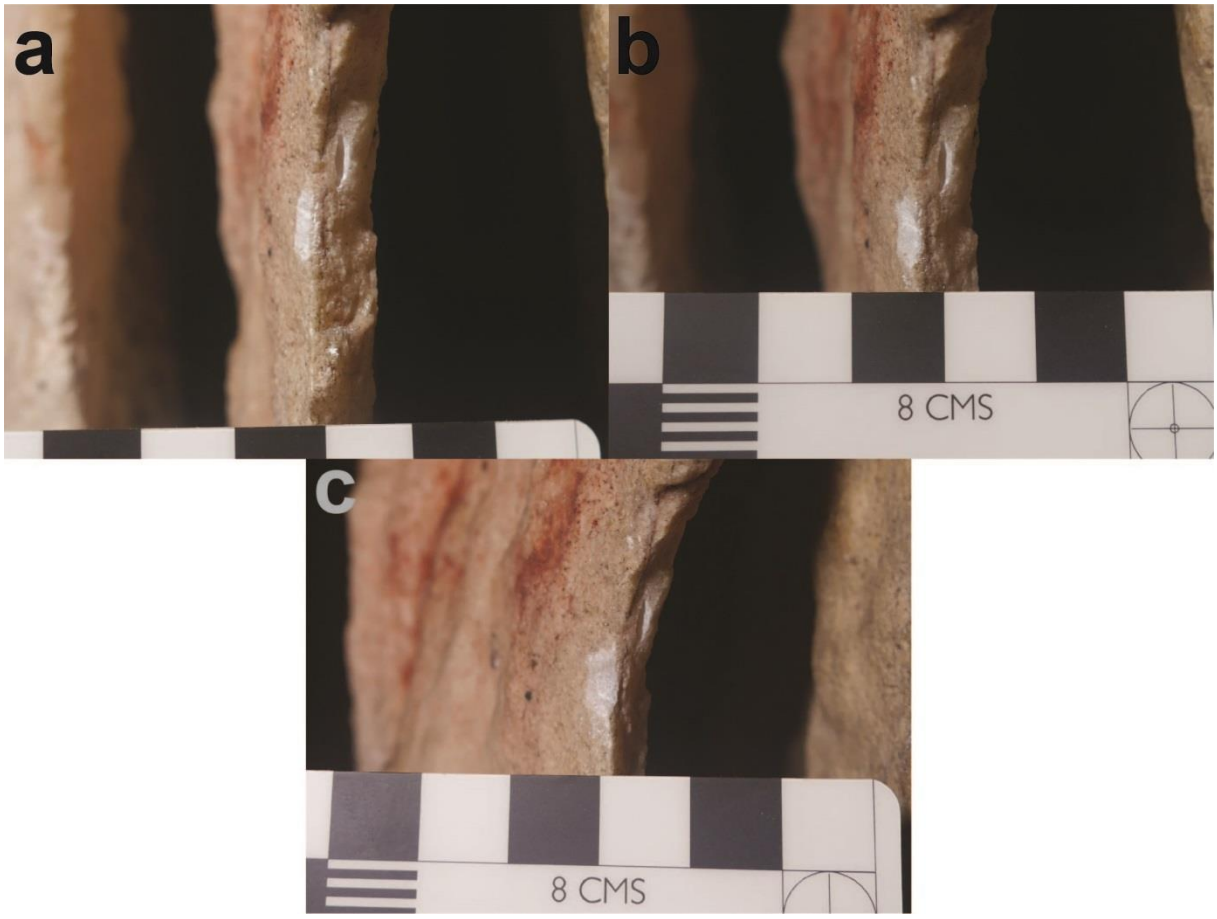

Fig. S32.

Details of sampling for ARD 15: (a) after cleaning, (b) after collecting sample ARD 15A, (c) after collecting sample ARD 15B. Note sample location of ARD 15 is located below and to the left of ARD 14, see also Fig. S31.

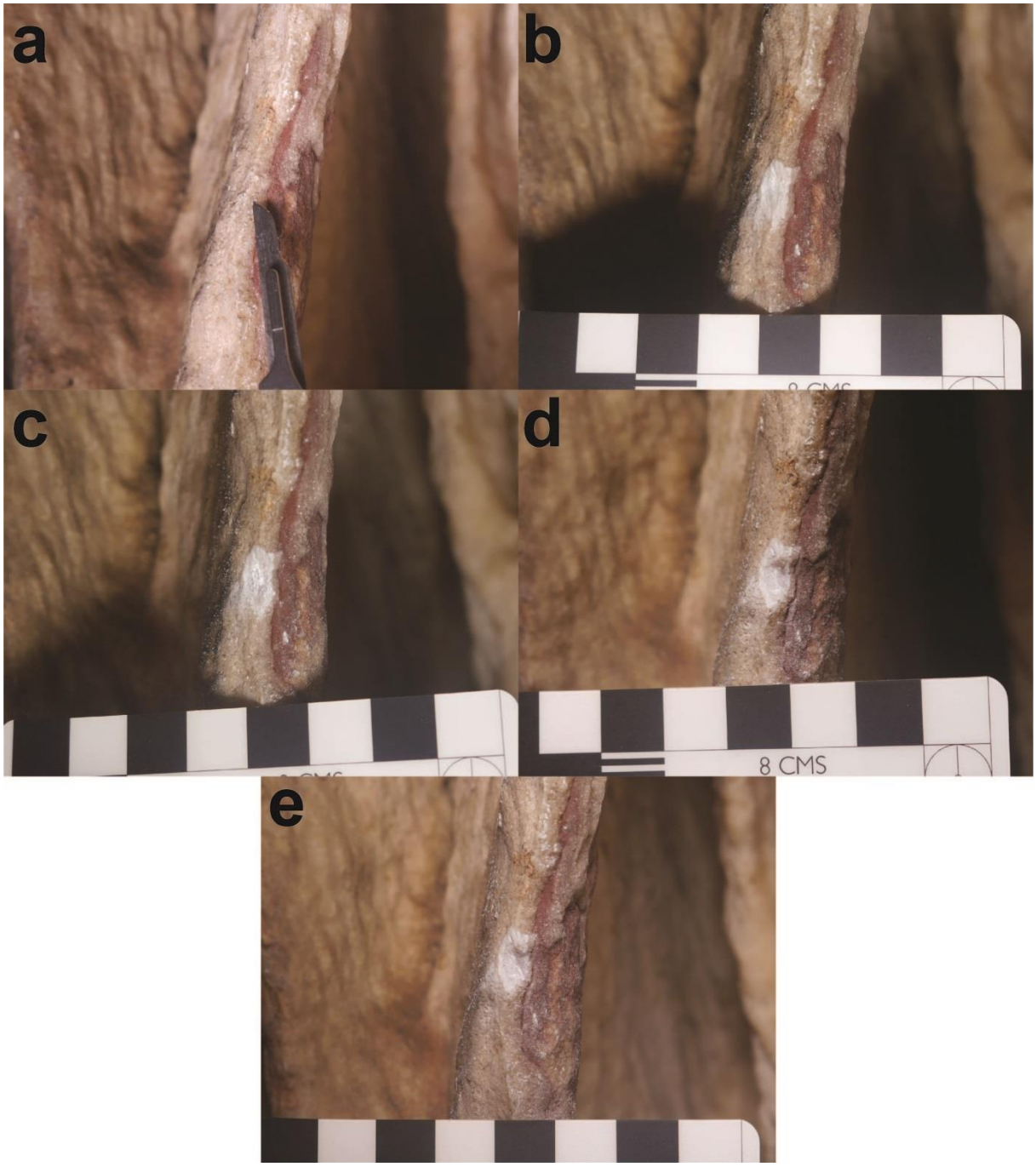

Fig. S33.

Details of sampling for ARD 16: (a) prior to sampling, (b) after cleaning, (c - e) after each sub-sample taken.

Fig. S34.

Detail of ARD 16 after sampling with pigment clearly visible under the carbonate.

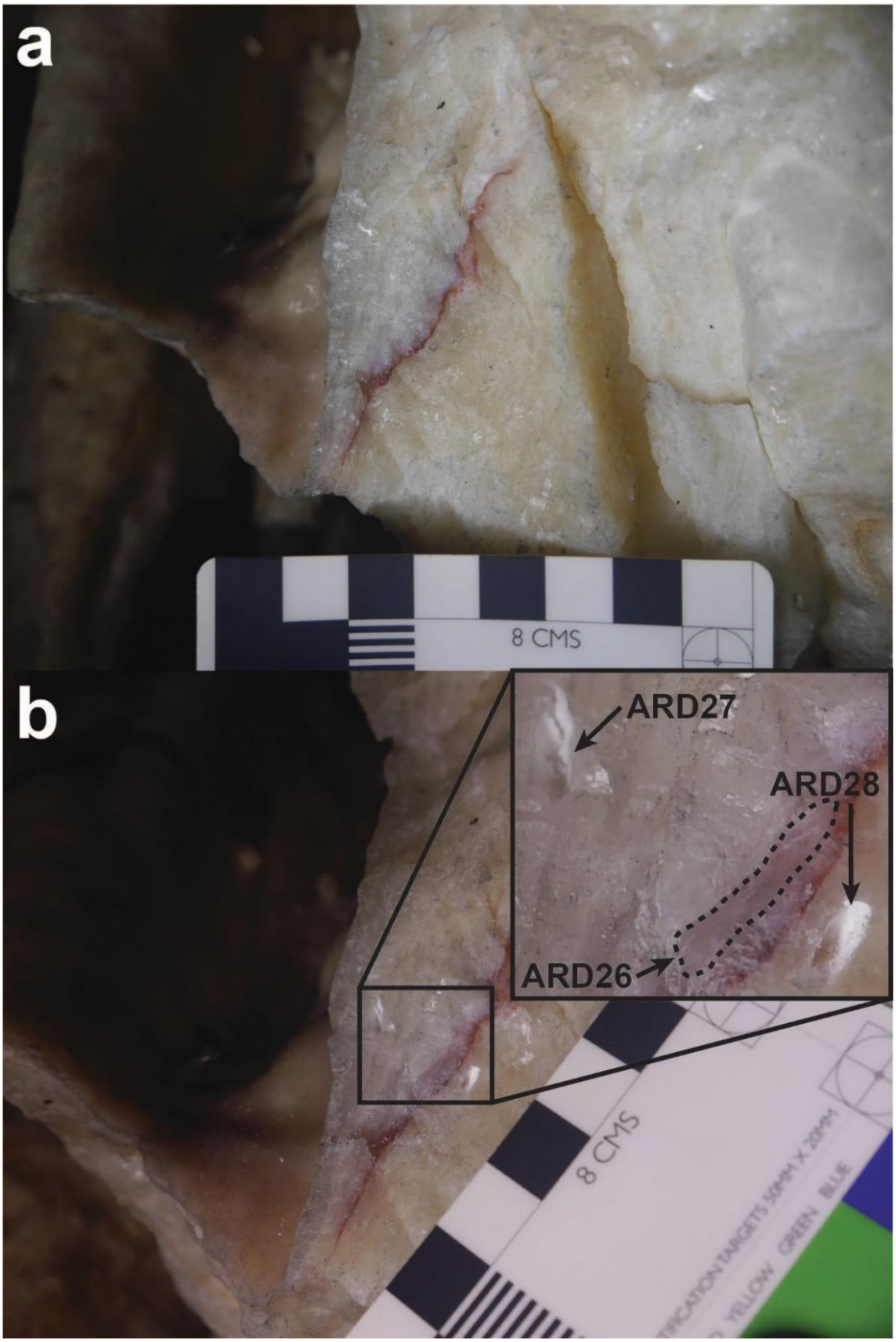

Fig. S35.

Sampling pigment on drapery between Panels III-C-2 and III-C-3, Ardales (ARD 26–28): (a) prior to sampling, (b) after sampling.

Fig. S36.

Panel II-C-8, Ardales. Surface of broken section of the curtain before sampling. The red painted exposed surface continues as a line of pigment visible in the broken drapery where it has been covered by subsequent calcite formation.

Fig S37.

Panel II-C-8, Ardales: curtain formation with red paint. Samples were drilled from the cross section exposed by a breakage. The insert indicates positions of samples ARD 6 to 10.

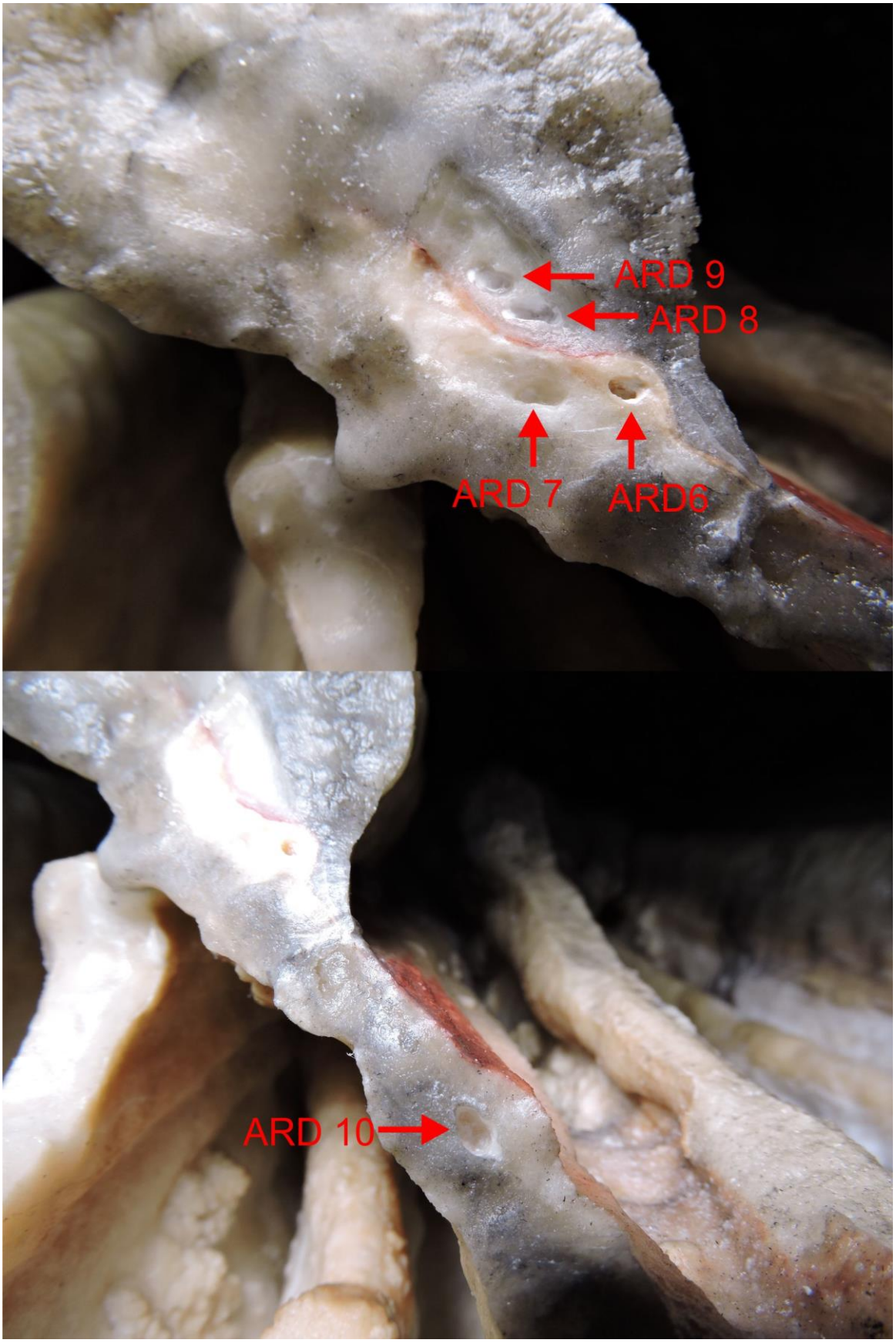

Fig S38.

Panel II-C-8, Ardales. Surface of broken section of the curtain after sampling. Top: Details of samples ARD 6 to 9. Bottom: Detail of sample ARD 10.

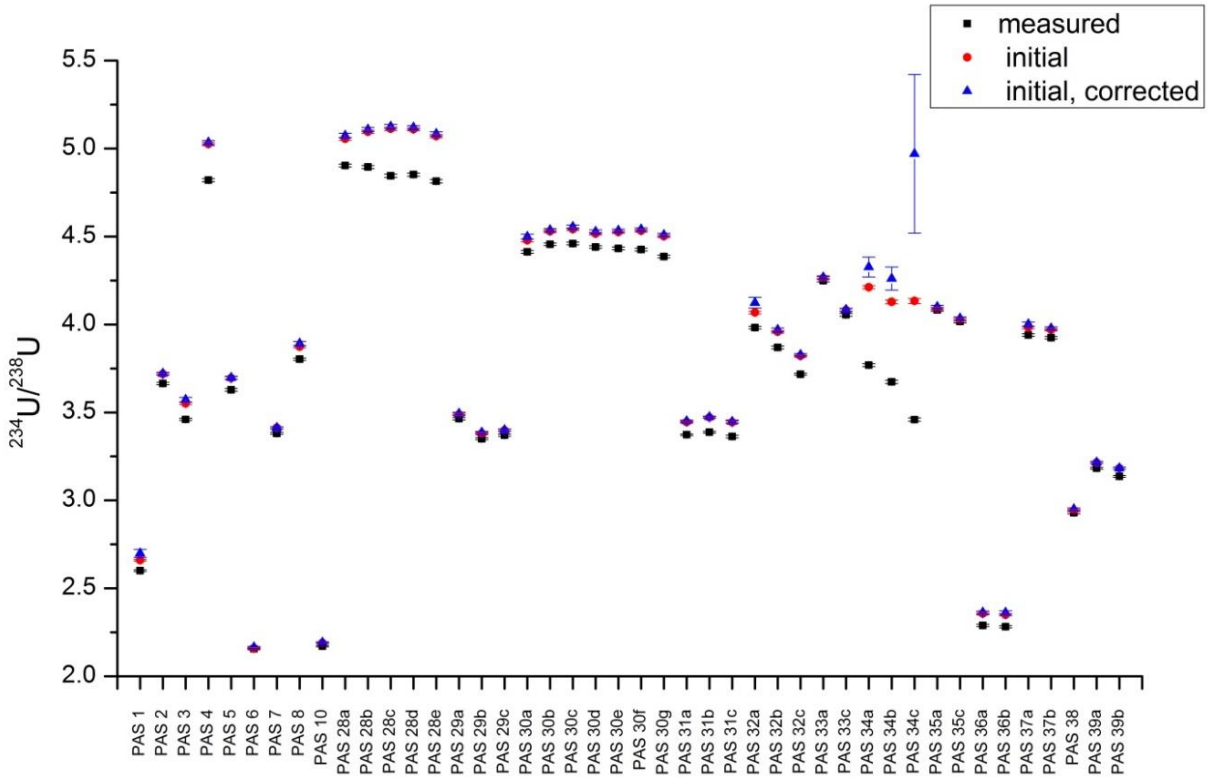

Fig. S39.

$^{234}U/^{238}U$ activity ratios for all samples from La Pasiega C ((*14*, *17*) and this study). Shown are the measured $^{234}U/^{238}U$ activity ratios and initial $^{234}U/^{238}U$ activity ratios calculated using both measured and corrected values of the $^{234}U/^{238}U$ activity ratio (correction factor 0.8 ± 0.4).

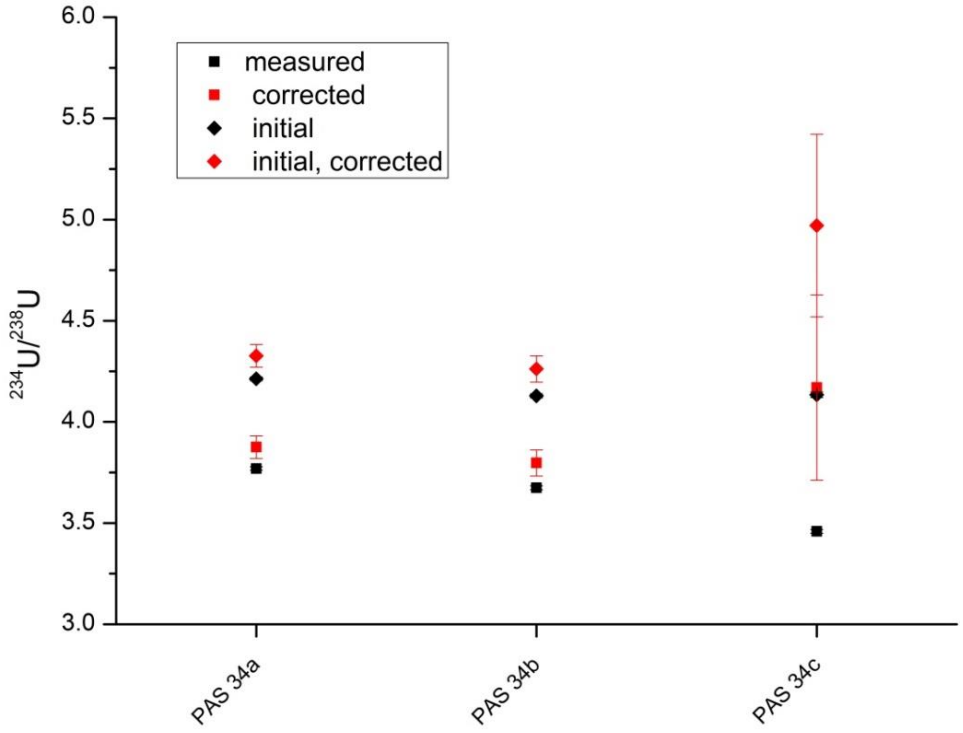

Fig. S40.

$^{234}U/^{238}U$ activity ratios for PAS 34 sub samples. Shown in black are the measured $^{234}U/^{238}U$ activity ratios and the initial $^{234}U/^{238}U$ activity ratios using the measured value to calculate an age. The same is shown in red for the corrected $^{234}U/^{238}U$ activity ratios, using a correction factor of 0.8 ± 0.4.

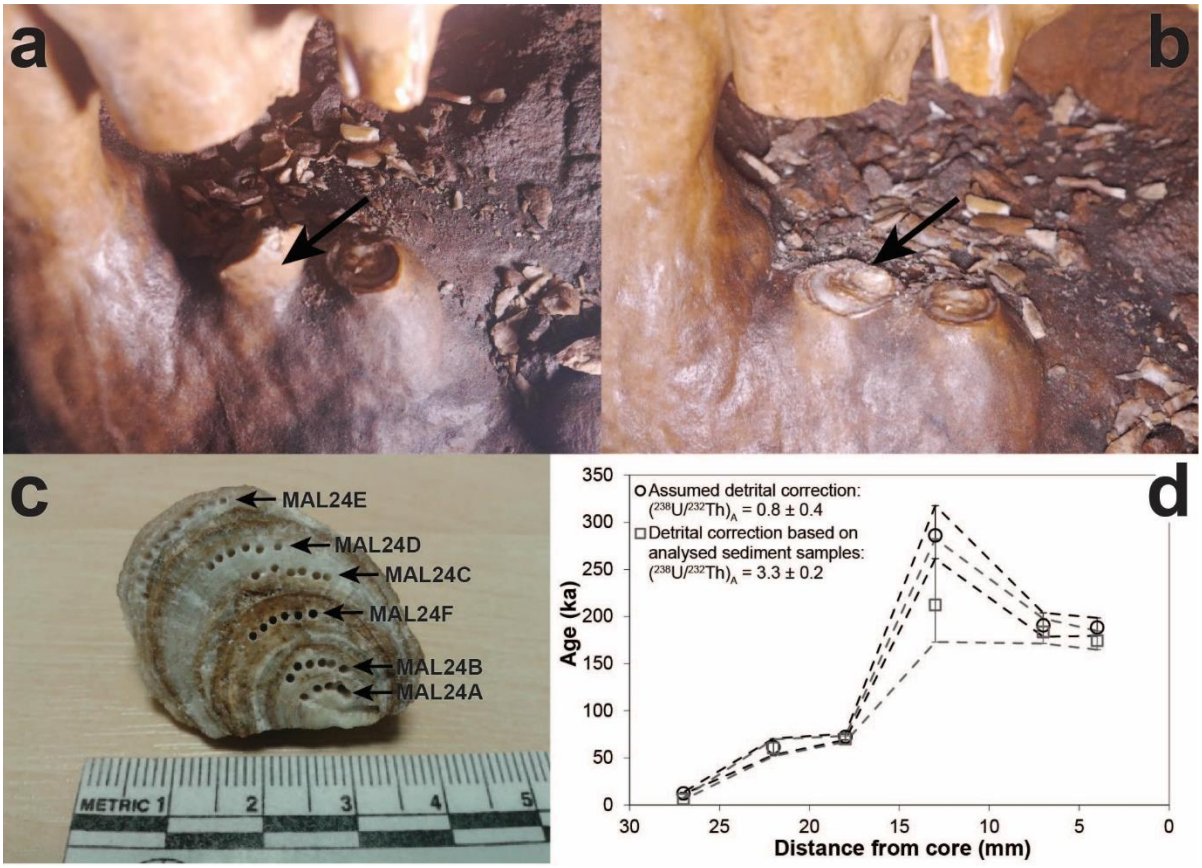

Fig. S41.

Sampling and dating the Maltravieso boss (MAL 24): (a) prior to sampling, (b) after sampling, (c) locations of the drilled sub-samples A–F (note that powders from multiple drill holes within each layer were combined to produce one dating sample per layer), (d) corrected U-Th ages for six carbonate sub-samples using i) an assumed detrital activity ratio of $^{238}U/^{232}Th = 0.8 \pm 0.4$ (black data labels) and ii) a measured (sediment) detrital activity ratio of $^{238}U/^{232}Th = 3.3 \pm 0.2$ (grey data labels); errors are fully propagated 2σ standard errors of the mean.

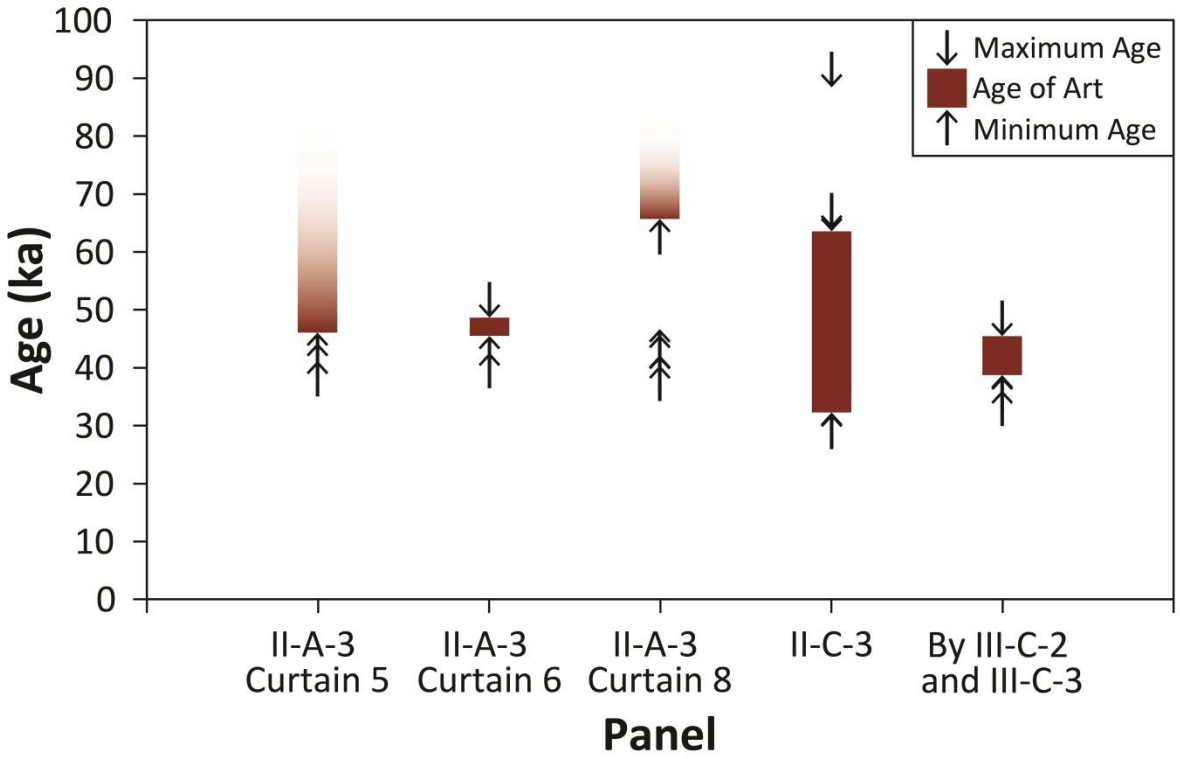

Fig. S42.

Summary of dating results from Ardales cave. The results show at least two discrete phases of painting.

Table S1.

U isotopic composition of standard solutions measured in MPI EVA. All ratios are concentration ratios.

Standard	$^{234}U/^{238}U$	$^{235}U/^{238}U$	$^{236}U/^{238}U$
REIMEP 18 A	$(5.6545 \pm 0.0049)\cdot10^{-5}$	$(7.2533 \pm 0.0036)\cdot10^{-3}$	$(2.9482 \pm 0.0133)\cdot10^{-8}$
certified value (39)	*$(5.6582 \pm 0.0041)\cdot10^{-5}$*	*$(7.2542 \pm 0.0036)\cdot10^{-3}$*	*$(3.0579 \pm 0.0083)\cdot10^{-8}$*
REIMEP 18 B	$(3.3292 \pm 0.0026)\cdot10^{-4}$	$3.5469 \pm 0.0012)\cdot10^{-2}$	$(3.8811 \pm 0.0030)\cdot10^{-4}$
certified value (39)	*$(3.3271 \pm 0.0022)\cdot10^{-4}$*	*$(3.5470 \pm 0.0018)\cdot10^{-2}$*	*$(3.8828 \pm 0.0013)\cdot10^{-4}$*
IRMM 183	$(1.9772 \pm 0.0020)\cdot10^{-5}$	$(3.2127 \pm 0.0032)\cdot10^{-3}$	$(1.4845 \pm 0.0011)\cdot10^{-4}$
certified value (40)	*$(1.9755 \pm 0.0022)\cdot10^{-5}$*	*$(3.2157 \pm 0.0016)\cdot10^{-3}$*	*$(1.4836 \pm 0.0005)\cdot10^{-4}$*
URAN 84.5	$(5.4891 \pm 0.0044)\cdot10^{-5}$	$(7.2565 \pm 0.0025)\cdot10^{-3}$	-

Table S2.

Th isotopic composition of standard solutions measured in MPI EVA. All ratios are concentration ratios.

Standard	$^{230}Th/^{229}Th$	$^{230}Th/^{232}Th$	$^{229}Th/^{232}Th$
TEDDi	1.519 ± 0.002	$(4.447 \pm 0.004)\cdot10^{-3}$	$(2.928 \pm 0.003)\cdot10^{-3}$
calibrated value (37)	*1.519 ± 0.002*	*$(4.444 \pm 0.007)\cdot10^{-3}$*	*$(2.927 \pm 0.005)\cdot10^{-3}$*
Thoca	0.2063 ± 0.0004	0.0613 ± 0.0002	0.297 ± 0.001
calibrated value	*0.2064 ± 0.0005*	*0.0613 ± 0.0003*	*0.297 ± 0.001*
Thosi	0.0947 ± 0.0002	$(1.1369 \pm 0.0026)\cdot10^{-5}$	$(1.2003 \pm 0.002)\cdot10^{-4}$
calibrated value	*0.0949 ± 0.0004*	*$(1.1369 \pm 0.003)\cdot10^{-5}$ (41)*	*$(1.1981 \pm 0.004)\cdot10^{-4}$*

Table S3.

U-Th ages for all Maltravieso speleothem samples using two different correction factors i) a bulk earth activity ratio of $^{238}U/^{232}Th = 0.8 \pm 0.4$ and ii) a measured (sediment) detrital activity ratio of $^{238}U/^{232}Th = 3.3 \pm 0.2$.

Sample ID	***Lab ID***	***Age corrected [ka]*** $(^{238}U/^{232}Th)_A = 0.8 \pm 0.4$	***Age corrected [ka]*** $(^{238}U/^{232}Th)_A = 3.3 \pm 0.2$
MAL13 Clean	UoS-UTh-A112	50.62 + 3.38 - 3.02	41.68 + 2.44 - 2.29
MAL 13A	UoS-UTh-A98	73.72 + 3.99 - 3.67	70.08 + 3.82 - 3.37
MAL 14A	UoS-UTh-A79	19.05 + 1.08 - 1.05	16.94 + 0.93 - 0.92
MAL 14B	UoS-UTh-A71	24.36 + 0.52 - 0.51	23.59 ± 0.47
MAL 14C	UoS-UTh-A80	22.82 + 1.15 - 1.09	22.35 + 1.10 - 1.14
MAL 15A	UoS-UTh-A178	23.39 + 2.46 - 2.5	20.66 + 2.46 - 2.44
MAL 15B	UoS-UTh-A133	18.53 + 1.75 - 1.69	16.92 + 1.74 - 1.70
MAL 15C	UoS-UTh-A179	15.7 + 1.77 - 1.72	15.29 + 1.79 - 1.74
MAL 15D	UoS-UTh-A134	17.53 + 0.48 - 0.48	17.15 + 0.45 - 0.46
MAL 15E	UoS-UTh-A180	20.01 + 0.57 - 0.57	18.37 + 0.38 - 0.39
MAL 15F	UoS-UTh-A135	42.39 + 4.58 - 4.26	39.48 + 4.45 - 4.21
MAL 17A	UoS-UTh-A148	15.48 + 1.43 - 1.4	14.18 + 1.38 - 1.40
MAL 17B	UoS-UTh-A150	18.79 + 1.49 - 1.54	15.3 + 1.21 - 1.24
MAL 17C	UoS-UTh-A171	43.91 + 2.27 - 2.3	37.25 + 1.73 - 1.70
MAL 17D	UoS-UTh-A151	68.04 + 9.37 - 8.87	63.63 + 9.60 - 8.39
MAL 19 Clean	UoS-UTh-A136	16.39 + 5.44 - 5.13	1.13 + 4.16 - 1.04
MAL 19A	UoS-UTh-A137	21.66 + 2.99 - 2.95	17.31 + 2.83 - 2.60
MAL 24A	UoS-UTh-A159	188.5 + 10.60 - 9.46	174.37 + 10.34 - 9.50
MAL 24B	UoS-UTh-A160	190.62 + 13.68 - 11.74	183.63 + 14.31 - 12.31
MAL 24F	UoS-UTh-A161	286.25 + 44.63 - 30.9	212.26 + 70.18 - 39.33
MAL 24C	UoS-UTh-A164	72.28 + 3.24 - 3.16	69.98 + 3.26 - 3.11
MAL 24D	UoS-UTh-A165	61.37 + 9.01 - 8.5	60.39 + 9.28 - 8.50
MAL 24E	UoS-UTh-A166	12.47 + 1.82 - 1.84	6.65 + 1.11 - 1.04

Table S4.

U-series results for La Pasiega C, Maltravieso and Ardales.

Spl ID	*Lab ID*	^{238}U [ng/g]	^{232}Th [ng/g]	$^{232}Th/^{238}U$	$^{230}Th/^{232}Th$	$^{230}Th/^{238}U$	$^{234}U/^{238}U$	*Age uncorrected* [ka]	^{234}
PAS 33a	UEVA 174	1205.36 ± 76.53	7.76 ± 0.51	0.0021 ± 0.00002	28.27 ± 0.76	0.0595 ± 0.0018	4.2495 ± 0.0078	1.54 ± 0.05	4.263
PAS 33c	UEVA 175	1799.10 ± 377.05	5.03 ± 1.01	0.0009 ± 0.000008	124.09 ± 1.85	0.1134 ± 0.0019	4.0552 ± 0.0077	3.09 ± 0.05	4.082
PAS 34a	UEVA 176	289.29 ± 9.06	40.81 ± 1.29	0.0461 ± 0.0001	32.82 ± 0.21	1.5149 ± 0.0106	3.7694 ± 0.0082	52.52 ± 0.47	4.212
PAS 34b	UEVA 309	215.56 ± 7.43	36.00 ± 1.22	0.0548 ± 0.0001	28.28 ± 0.19	1.5453 ± 0.0121	3.6744 ± 0.0094	55.53 ± 0.56	4.128
PAS 34c	UEVA 177	178.31 ± 8.31	152.93 ± 7.10	0.2803 ± 0.0006	7.25 ± 0.07	2.0348 ± 0.0213	3.4591 ± 0.0092	85.79 ± 1.28	4.133
PAS 35a	BIG-UTh-A 1282	747.99 ± 35.55	9.54 ± 0.48	0.0042 ± 0.00004	7.51 ± 0.27	0.0314 ± 0.0012	4.0833 ± 0.0077	0.84 ± 0.03	4.090
PAS 35c	BIG-UTh-A 1283	508.65 ± 11.64	4.62 ± 0.13	0.0030 ± 0.00003	14.59 ± 0.34	0.0434 ± 0.0012	4.0177 ± 0.0080	1.18 ± 0.03	4.027
PAS 36a	UEVA 178	108.99 ± 2.88	2.40 ± 0.06	0.0072 ± 0.00005	48.57 ± 0.78	0.3507 ± 0.0053	2.2893 ± 0.0067	17.88 ± 0.29	2.356
PAS 36b	UEVA 179	103.82 ± 1.73	4.16 ± 0.08	0.0131 ± 0.00008	27.08 ± 0.41	0.3551 ± 0.0049	2.2819 ± 0.0063	18.19 ± 0.27	2.349
PAS 37a	UEVA 182	504.87 ± 11.86	12.87 ± 0.31	0.0083 ± 0.00004	21.86 ± 0.18	0.1823 ± 0.0015	3.9407 ± 0.0071	5.14 ± 0.04	3.983
PAS 37b	UEVA 183	572.25 ± 14.24	6.16 ± 0.16	0.0035 ± 0.00002	54.67 ± 0.60	0.1927 ± 0.0019	3.9250 ± 0.0072	5.46 ± 0.06	3.970
PAS 38	UEVA 184	818.24 ± 38.55	13.62 ± 0.60	0.0054 ± 0.00003	11.36 ± 0.19	0.0619 ± 0.0010	2.9292 ± 0.0060	2.33 ± 0.04	2.941
PAS 39a	UEVA 185	947.23 ± 16.41	2.57 ± 0.05	0.0009 ± 0.000005	166.11 ± 1.23	0.1476 ± 0.0010	3.1821 ± 0.0054	5.16 ± 0.04	3.214
PAS 39b	UEVA 186	1041.25 ± 24.11	0.62 ± 0.02	0.0002 ± 0.000001	1091.00 ± 9.13	0.2110 ± 0.0013	3.1364 ± 0.0054	7.55 ± 0.05	3.182
ARD 06	UEVA 955	511.42 ± 6.38	20.85 ± 0.25	0.0134 ± 0.00003	34.95 ± 0.14	0.4661 ± 0.0021	1.0459 ± 0.0021	64.09 ± 0.44	1.055
ARD 07	UEVA 956	244.34 ± 2.62	1.85 ± 0.02	0.0025 ± 0.00001	231.17 ± 1.60	0.5728 ± 0.0029	1.0314 ± 0.0023	88.01 ± 0.77	1.040

ARD 08	UEVA 957	297.21 ± 2.89	1.69 ± 0.02	0.0019 ± 0.00001	145.58 ± 1.06	0.2703 ± 0.0018	1.0477 ± 0.0024	32.51 ± 0.26	1.052
ARD 09	UEVA 958	298.83 ± 2.67	1.78 ± 0.02	0.0020 ± 0.00001	138.12 ± 0.95	0.2690 ± 0.0014	1.0430 ± 0.0022	32.50 ± 0.22	1.047
ARD 10	UEVA 1005	182.17 ± 3.27	1.80 ± 0.03	0.0032 ± 0.00002	141.85 ± 1.42	0.4577 ± 0.0039	1.0338 ± 0.0036	63.60 ± 0.81	1.040
ARD 12A	UoS-UTh-A245	509.8 ± 5.04	4.20 ± 0.04	0.002698 ± 0.000017	134.23 ± 0.96	0.3622 ± 0.0034	1.0394 ± 0.0026	46.64 + 0.57 - 0.55	1.044
ARD 12A repeat	UoS-UTh-A284	511.25 ± 5.43	4.05 ± 0.05	0.002592 ± 0.000016	139.06 ± 0.89	0.3605 ± 0.0035	1.0386 ± 0.0038	46.41 + 0.63 - 0.58	1.044
ARD 12B	UoS-UTh-A246	244.8 ± 2.83	3.71 ± 0.05	0.004957 ± 0.000029	68.27 ± 0.6	0.3384 ± 0.0033	1.0366 ± 0.0039	43.04 ± 0.55	1.041
ARD 12C	UoS-UTh-A236	207.5 ± 3.32	3.73 ± 0.06	0.005877 ± 0.000084	57.42 ± 1.23	0.3374 ± 0.0082	1.0319 ± 0.0386	43.15 + 2.68 - 2.37	1.036
ARD 12D	UoS-UTh-A237	214.88 ± 8.90	4.22 ± 0.19	0.006427 ± 0.000108	53.69 ± 1.37	0.3450 ± 0.0110	1.0320 ± 0.0147	44.33 + 1.92 - 1.89	1.036
ARD 13A	UoS-UTh-A222	1229.61 ± 25.84	9.00 ± 0.19	0.002396 ± 0.000014	152.83 ± 1.14	0.3661 ± 0.0033	1.0385 ± 0.0033	47.33 + 0.57 - 0.56	1.044
ARD 13B	UoS-UTh-A223	331.54 ± 13.53	11.60 ± 0.44	0.011452 ± 0.000070	42.59 ± 0.58	0.4878 ± 0.0073	1.0369 ± 0.0234	69.09 + 2.93 - 2.62	1.044
ARD 14A	UoS-UTh-A231	684.76 ± 13.29	1.95 ± 0.04	0.000932 ± 0.000012	395.03 ± 4.91	0.3683 ± 0.0063	1.0379 ± 0.0029	47.72 + 1.05 - 1.02	1.043
ARD 15A	UoS-UTh-A232	1696.03 ± 53.88	5.51 ± 0.20	0.001063 ± 0.000011	337.14 ± 3.63	0.3584 ± 0.0050	1.0374 ± 0.0025	46.15 + 0.81 - 0.82	1.042
ARD 15B	UoS-UTh-A233	667.98 ± 37.85	4.65 ± 0.29	0.002280 ± 0.000043	152.07 ± 3.27	0.3467 ± 0.0110	1.0347 ± 0.0061	44.45 + 1.79 - 1.82	1.039
ARD 16A	UoS-UTh-A247	313.84 ± 5.88	5.40 ± 0.11	0.005629 ± 0.000031	58.92 ± 0.74	0.3317 ± 0.0044	1.0323 ± 0.0051	42.23 + 0.74 - 0.72	1.036
ARD 16B	UoS-UTh-A248	250.2 ± 4.29	3.29 ± 0.07	0.004306 ± 0.000036	84.25 ± 0.84	0.3628 ± 0.0050	1.0314 ± 0.0051	47.23 + 0.85 - 0.83	1.035
ARD 16C	UoS-UTh-A249	227.59 ± 28.55	4.53 ± 0.58	0.006509 ± 0.000172	56.70 ± 2.84	0.3690 ± 0.0213	1.0227 ± 0.0342	48.79 + 4.26 - 4.00	1.026
ARD 26A	UoS-UTh-A238	564.64 ± 13.56	0.56 ± 0.02	0.000323 ± 0.000010	1004.53 ± 20.81	0.3243 ± 0.0099	1.0502 ± 0.0203	40.20 + 1.84 - 1.69	1.056
ARD 26B	UoS-UTh-A239	532.37 ± 14.02	0.54 ± 0.02	0.000330 ± 0.000011	985.93 ± 24.33	0.3258 ± 0.0112	1.0496 ± 0.0113	40.45 + 1.82 - 1.70	1.055
ARD 27A	UoS-UTh-A240	491.08 ± 7.58	0.46 ± 0.01	0.000303 ± 0.000006	1002.62 ± 26.5	0.3040 ± 0.0087	1.0481 ± 0.0068	37.30 + 1.32 - 1.31	1.053
ARD 28A	UoS-UTh-A241	520.54 ± 8.11	0.12 ± 0.01	0.000073 ± 0.000004	4626.61 ± 188.57	0.3379 ± 0.0192	1.0458 ± 0.0124	42.48 + 3.09 - 2.91	1.051

MAL 13 Clean	UoS-UTh-A112	117.2 ± 1.99	13.32 ± 0.21	0.037192 ± 0.000233	12.47 ± 0.16	0.4639 ± 0.0068	1.1872 ± 0.0328	53.32 + 2.30 - 2.13	1.217
MAL 13A	UoS-UTh-A98	142.69 ± 3.39	7.05 ± 0.21	0.016177 ± 0.000189	37.50 ± 0.57	0.6067 ± 0.0123	1.2024 ± 0.0305	74.86 + 3.78 - 3.41	1.250
MAL 14A	UoS-UTh-A79	209.87 ± 2.41	5.93 ± 0.08	0.009244 ± 0.000058	21.65 ± 0.88	0.2001 ± 0.0078	1.2059 ± 0.0067	19.71 + 0.84 - 0.83	1.217
MAL 14B	UoS-UTh-A71	287.55 ± 4.39	3.05 ± 0.11	0.003467 ± 0.000126	71.64 ± 2.33	0.2484 ± 0.0037	1.2236 ± 0.0088	24.60 ± 0.45	1.239
MAL 14C	UoS-UTh-A80	439.04 ± 8.30	2.87 ± 0.07	0.002142 ± 0.000038	109.67 ± 4.91	0.2349 ± 0.0102	1.2308 ± 0.0071	22.97 + 1.11 - 1.14	1.246
MAL 15A	UoS-UTh-A178	168.69 ± 6.85	6.18 ± 0.40	0.011997 ± 0.000622	20.26 ± 1.47	0.2430 ± 0.0213	1.2135 ± 0.0052	24.24 + 2.48 - 2.32	1.228
MAL 15B	UoS-UTh-A133	299.61 ± 7.02	6.55 ± 0.16	0.007157 ± 0.000102	27.39 ± 2.11	0.1960 ± 0.0158	1.2195 ± 0.0161	19.04 + 1.71 - 1.66	1.231
MAL 15C	UoS-UTh-A179	490.44 ± 11.16	2.77 ± 0.22	0.001849 ± 0.000123	89.93 ± 6.52	0.1663 ± 0.0170	1.2268 ± 0.0029	15.83 + 1.71 - 1.70	1.237
MAL 15D	UoS-UTh-A134	791.42 ± 10.52	4.19 ± 0.08	0.001730 ± 0.000020	106.56 ± 2.04	0.1844 ± 0.0044	1.2295 ± 0.0042	17.65 + 0.45 - 0.46	1.241
MAL 15E	UoS-UTh-A180	519.3 ± 11.49	11.58 ± 0.26	0.007299 ± 0.000038	28.84 ± 0.3	0.2105 ± 0.0028	1.2220 ± 0.0024	20.53 + 0.30 - 0.29	1.235
MAL 15F	UoS-UTh-A135	286.89 ± 11.69	10.83 ± 0.47	0.012350 ± 0.000212	31.12 ± 2.6	0.3843 ± 0.0300	1.1642 ± 0.0328	43.30 + 4.65 - 4.23	1.185
MAL 17A	UoS-UTh-A148	301.46 ± 5.79	5.36 ± 0.13	0.005814 ± 0.000088	28.69 ± 2.21	0.1668 ± 0.0132	1.2268 ± 0.0037	15.89 + 1.36 - 1.35	1.237
MAL 17B	UoS-UTh-A150	304.45 ± 5.37	14.46 ± 0.26	0.015545 ± 0.000111	13.33 ± 0.6	0.2072 ± 0.0104	1.2383 ± 0.0035	19.88 + 1.09 - 1.08	1.252
MAL 17C	UoS-UTh-A171	243.68 ± 6.90	21.04 ± 0.73	0.028253 ± 0.000383	14.66 ± 0.33	0.4141 ± 0.0100	1.1936 ± 0.0038	45.95 + 1.37 - 1.35	1.220
MAL 17D	UoS-UTh-A151	190.44 ± 9.22	10.52 ± 0.56	0.018068 ± 0.000357	29.68 ± 2.97	0.5362 ± 0.0496	1.1278 ± 0.0075	69.42 + 9.12 - 8.62	1.155
MAL 19 Clean	UoS-UTh-A136	109.03 ± 1.82	19.96 ± 0.36	0.059902 ± 0.000375	3.47 ± 0.43	0.2079 ± 0.0257	1.1916 ± 0.0288	20.83 + 2.89 - 2.83	1.203
MAL 19A	UoS-UTh-A137	199.77 ± 4.78	11.56 ± 0.29	0.018932 ± 0.000174	12.25 ± 1.26	0.232 ± 0.0237	1.2140 ± 0.0239	23.02 + 2.68 - 2.64	1.228
MAL 24A	UoS-UTh-A159	121.05 ± 1.56	19.94 ± 0.25	0.053889 ± 0.000296	17.11 ± 0.29	0.9218 ± 0.0169	1.0914 ± 0.0032	192.65 + 10.07 - 8.82	1.157
MAL 24B	UoS-UTh-A160	101.8 ± 1.45	8.83 ± 0.12	0.028376 ± 0.000195	32.74 ± 0.73	0.9292 ± 0.0228	1.0984 ± 0.0040	192.76 + 13.39 - 12.24	1.169
MAL 24F	UoS-UTh-A161	145.5 ± 1.72	87.71 ± 1.14	0.197236 ± 0.001066	5.25 ± 0.07	1.0353 ± 0.0148	1.0797 ± 0.0031	301.88 + 23.92 - 20.38	1.187

MAL 24C	UoS-UTh-A164	127.6 ± 1.52	3.62 ± 0.08	0.009274 ± 0.000194	58.22 ± 1.33	0.5400 ± 0.0167	1.0980 ± 0.0028	73 + 3.24 - 3.23	1.120
MAL 24D	UoS-UTh-A165	62.98 ± 0.70	0.79 ± 0.06	0.004096 ± 0.000292	120.16 ± 9.03	0.4922 ± 0.0526	1.1297 ± 0.0039	61.68 + 9.02 - 8.33	1.154
MAL 24E	UoS-UTh-A166	158.53 ± 2.12	11.99 ± 0.21	0.024738 ± 0.000227	5.99 ± 0.18	0.1482 ± 0.0044	1.2060 ± 0.0028	14.26 + 0.44 - 0.45	1.214
MAL Sed1	UoS-UTh-A184 UoS-UTh-A189			0.285538 ± 0.001520				n.a.	
MAL Sed2	UoS-UTh-A185 UoS-UTh-A190			0.313206 ± 0.001536				n.a.	
MAL Sed3	UoS-UTh-A186 UoS-UTh-A191			0.304691 ± 0.001520				n.a.	

All ratios are activity ratios. Analytical errors are at 95 % confidence level.

Age calculation is based on $\left(\frac{^{230}Th}{^{238}U}\right)(T) = (1 - e^{-\lambda_{230} T}) + \left(\left(\frac{^{234}U}{^{238}U}\right)(T) - 1\right)\frac{\lambda_{230}}{\lambda_{230} - \lambda_{234}}(1 - e^{-(\lambda_{230} - \lambda_{234}) T})$ where

T is the age of the sample.

The degree of detrital ^{230}Th contamination is indicated by the measured ^{230}Th/^{232}Th activity ratio and corrections were calculated using a ^{238}U/^{232}Th activity ratio of 0.8 ± 0.4, except for samples from Maltravieso (MAL) for which a correction factor of 3.3 ± 0.4 is applied.

^{234}U/^{238}U$_{ini}$ is the initial ^{234}U/^{238}U activity ratio.